UV Photoelectron and ab Initio Quantum Mechanical Evaluation of Nucleotide Ionization Potentials in Water−Counterion Environments: π Polarization Effects on DNA Alkylation by Carcinogenic Methylating Agents

Nancy S. Kim and Pierre R. LeBreton*

Contribution from the Department of Chemistry, The University of Illinois at Chicago, Chicago, Illinois 60607-7061

Received October 16, 1995[⊗]

Abstract: Gas-phase ionization potentials (IPs) were evaluated for anionic 2′-deoxyguanosine 5′-phosphate (5′-dGMP$^-$) and for 5′-dGMP$^-$ in water, counterion clusters with Na^+. Gas-phase IPs of isolated 5′-dGMP$^-$ and of 5′-dGMP$^-$ in clusters containing Na^+ and 4, 8, 11, 12, and 14 water molecules, obtained from ab initio self-consistent field (SCF) molecular orbital calculations, were corrected by employing gas-phase UV photoelectron data on the model compounds 1,9-dimethylguanine, 3-hydroxytetrahydrofuran, and water together with results from second-order Möller−Plesset and configuration interaction singles calculations on the model anion $CH_3HPO_4^-$. The correction procedure depends on results from recent investigations (Kim, H. S.; Yu, M.; Jiang, Q.; LeBreton, P. R. *J. Am. Chem. Soc.* **1993**, *115*, 6169−6183. Kim, H. S.; LeBreton, P. R. *Proc. Natl. Acad. Sci. U.S.A.* **1994**, *91*, 3725−3729), which indicate that the upper occupied nucleotide valence orbitals described by SCF calculations with split valence basis sets are largely localized on the base, sugar, or phosphate groups. In the gas-phase, the nucleotide environment strongly influences the IPs. For the gas-phase cluster 5′-dGMP$^-$·14H_2O·Na^+ (cluster **I**), in which Na^+ is bound to phosphate, the lowest energy base, sugar, and phosphate IPs are 2.2, 2.3, and 3.7 eV smaller than corresponding IPs in 5′-dGMP$^-$ without H_2O or Na^+, and the energetic ordering of IPs is different. In 5′-dGMP$^-$, the lowest energy base IP (5.8 eV) is 0.4 eV larger than that of the phosphate group. In cluster **I**, the base IP (8.0 eV) is 1.1 eV smaller than that of the phosphate group. Gibbs free energies associated with ionization in aqueous solution (ΔG_{ioniz}(solution)) were obtained by adding the difference ($\Delta\Delta G_{hyd}$) between the hydration energies of 5′-dGMP$^-$ or of the 5′-dGMP$^-$ clusters, before and after ionization, to the corrected gas phase IPs: ΔG_{ioniz}(solution) $\approx$ IP + $\Delta\Delta G_{hyd}$. Differences between corresponding values of ΔG_{ioniz}(solution) for ionization from 5′-dGMP$^-$ versus 5′-dGMP$^-$ in clusters are smaller than differences between gas-phase IPs. In cluster **I**, values of ΔG_{ioniz}-(solution) for the lowest energy base and phosphate ionization events (6.7 and 8.3 eV, respectively) are 0.1 and 0.9 eV larger than for 5′-dGMP$^-$. In the cluster, the lowest sugar ionization energy (8.6 eV) is 0.3 eV smaller than in 5′-dGMP$^-$. Nucleotide reactivities toward the carcinogen, *N*-methyl-*N*-nitrosourea, which methylates DNA via a reactive methane diazonium ion ($CH_3N_2^+$), increase as nucleotide base π ionization potentials decrease. Employing transition-state geometries obtained from semiempirical MNDO calculations for gas-phase reactions of $CH_3N_2^+$ with nucleoside model compounds (9-methylguanine, 9-methyladenine, 1-methylcytosine, and 1-methylthymine), results from single-point ab initio 4-31G and 6-31G SCF calculations provide evidence that the activation barriers are strongly influenced by hydration, and that nucleotide base π polarization effects, modulated by steric interactions, play an important role in determining DNA methylation patterns.

Introduction

The electronic structure of nucleotides plays a central role in the chemistry and biology of DNA. Electronic investigations of nucleotide components and nucleotide base model compounds have been carried out in order to better understand DNA reactivity with electrophilic mutagens and carcinogens,[1−3] base tautomerism,[4−6] base hydrogen bonding and solvation,[7] proton transfer in radical base anions,[8] and radiation-induced DNA damage.[9] The recent discovery of long-range photoinduced electron transfer further demonstrates the influence of electronic structure on the physical properties of DNA.[10,11] Most descriptions of the electronic structures of nucleotide components[4,5,6,7,9,12,13] and nucleotide model compounds[1,3] rely on results from theoretical descriptions obtained from molecular orbital calculations. Because of the complexity of nucleotides, computational descriptions are greatly aided by spectroscopic markers which can be used to test and correct the theoretical results.[4,5,6,14,15]

[⊗] Abstract published in *Advance ACS Abstracts,* April 1, 1996.

(1) Ford, G. P.; Scribner, J. D. *J. Am. Chem. Soc.* **1983,** *105*, 349.
(2) Ford, G. P.; Scribner, J. D. *Chem. Res. Toxicol.* **1990,** *3*, 219.
(3) Pardo, L.; Osman, R.; Weinstein, H.; Rabinowitz, J. R. *J. Am. Chem. Soc.* **1993**, *115*, 8263.
(4) Person, W. B.; Szczepaniak, K. In *Vibrational Spectra and Structure*; Durig, J. R., Ed.; Elsevier Science Publishers B.V.: Amsterdam, The Netherlands, 1993; Vol. 20, pp 239−325.
(5) Szczepaniak, K.; Szczesniak, M. *J. Mol. Struct.* **1987**, *156*, 29.
(6) Szczesniak, M.; Szczepaniak, K.; Kwiatkowski, J. S.; KuBulat, K.; Person, W. B. *J. Am. Chem. Soc.* **1988**, *110*, 8319.
(7) Young, P. E.; Hiller, lan H.; Gould, lan R. *J. Chem. Soc., Perkin Trans. 2* **1994**, 1717.
(8) Colson, A.-O.; Besler, B.; Close, D. M.; Sevilla, M. D. *J. Phys. Chem.* **1992**, *96*, 661.
(9) Colson, A.-O.; Sevilla, M. D. *J. Phys. Chem.* **1995**, *99*, 3867.
(10) Murphy, C. J.; Arkin, M. R.; Jenkins, Y.; Ghatlia, N. D.; Bossmann, S. H.; Turro, N. J.; Barton, J. K. *Science* **1993**, *262*, 1025.
(11) Risser, S. M.; Beratan, D. N. *J. Am. Chem. Soc.* **1993**, *115*, 2508.
(12) Colson, A. -O.; Besler, B.; Sevilla, M. D. *J. Phys. Chem.* **1993**, *97*, 8092.
(13) Sevilla, M. D.; Besler, B.; Colson, A.-O. *J. Phys. Chem.* **1995**, *99*, 1060.

0002-7863/96/1518-3694$12.00/0

In recent investigations,[16−19] the combination of HeI UV photoelectron (PE) data for nucleotide model compounds, of results from ab initio self-consistent field (SCF) calculations on intact nucleotides, and of results from post-SCF calculations on phosphorus- and oxygen-containing model anions has provided descriptions of electron distributions and experimentally based valence electron ionization potentials (IPs) for 11 and 12 of the highest occupied molecular orbitals in 2′-deoxycytidine 5′-phosphate (5′-dCMP$^-$)[18] and 2′-deoxyguanosine 5′-phosphate (5′-dGMP$^-$),[16,17,19] respectively. This approach relies on the localized valence structure of nucleotides, in which the upper occupied orbitals reside primarily on either the base, sugar, or phosphate groups, and on the correlation of nucleotide valence orbitals with orbitals in the model compounds and anions.

Early evaluations of nucleotide valence IPs were restricted to isolated anions.[16−18,20] Recently, small nucleotide−water−counterion clusters containing 5′-dGMP$^-$, Na^+, and four water molecules were examined;[19] however, in the study of nucleotide clusters bulk solvent polarization effects were not considered. In the present investigation, PE data and results from molecular orbital and dipole relaxation theory were used to examine bulk solvent polarization effects on the ionization of clusters of 5′-dGMP$^-$ containing Na^+ and 4, 8, 11, 12, and 14 water molecules. The largest of these systems contains 79 atoms and 330 electrons. The results have been further employed to examine solvent and electronic influences on methanediazonium ion ($CH_3N_2^+$) reactions with DNA, which current evidence indicates play a central role in genotoxic mechanisms involving carcinogenic *N*-methyl-*N*-nitrosourea,[21] *N*-methyl-*N*′-nitro-*N*-nitrosoguanidine,[22] and 1,3,3-trimethyltriazene.[23]

Water−Counterion Environment of DNA. An understanding of water and Na^+ influences on nucleotide electronic structure is complicated by the dynamic nature of the interactions which occur on a picosecond time scale[24−27] and cannot be fully represented by a single structure. Here, we have examined cluster geometries in which a partially solvated Na^+ ion binds to the phosphate group of 5′-dGMP$^-$. The structure of the largest complex examined, cluster **I**, is shown in Figure 1. This cluster contains 14 water molecules, 9 of which are associated with hydration of the Na^+−phosphate ion pair.

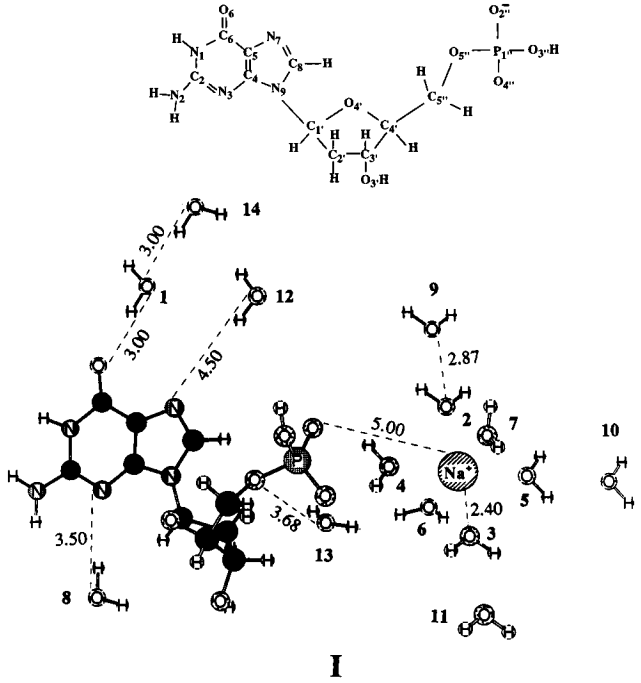

I

Figure 1. Structure of cluster **I** containing 5′-dGMP$^-$, Na^+, and 14 water molecules. All distances are given in angstroms.

Results from several experimental and theoretical investigations provide evidence that this structure is statistically significant. X-ray data for oligomeric DNA indicate that phosphate groups are principal[28−30] hydration sites. The strong hydration of the phosphate group is supported by IR measurements of evaporated DNA films at varying relative humidities.[31] Circular dichroism,[32] Raman,[33] IR,[34] and sedimentation[35] data and solvent accessibility surface area calculations[36] provide evidence that each nucleotide is closely associated with 10−15 water molecules. Crystallographic data for the B-DNA dodecamer CGCGAATTCGCG indicate the presence of structured water in the minor groove.[28b] However, analysis of the structures of nine other oligonucleotides of B-DNA shows that, on average, hydration of the major grove is greater than that of the minor groove.[37] Crystallographic data[37] for hydrated oligonucleotides indicate that for each nucleotide there are generally 1 or 2 structured water molecules located within 5 Å of each base, and 1 to 3 structured water molecules located within 5 Å of each phosphate group.[28,37] For oligomers containing guanine, water molecules bound to the O^6 or N7 base positions are generally more structured than water molecules bound to phosphate.[28,29,37]

In X-ray data from oligomers of B-DNA grown in solution with metal counterions, the counterion positions have not been

(14) Urano, S.; Yang, X.; LeBreton, P. R. *J. Mol. Struct.* **1989**, *214*, 315.
(15) (a) Padva, A.; LeBreton, P. R.; Dinerstein, R. J.; Ridyard, J. N. A. *Biochem. Biophys. Res. Commun.* **1974**, *60*, 1262. (b) Lauer, G.; Shafer, W.; Schweig, A. *Tetrahedron Lett.* **1975**, *45*, 3939. (c) Hush, N. S.; Cheung, A. S. *Chem. Phys. Lett.* **1975**, *34*, 11. (d) Padva, A.; O'Donnell, T. J.; LeBreton, P. R. *Chem. Phys. Lett.* **1976**, *41*, 278. (e) Dougherty, D.; Wittel, K.; Meeks, J.; McGlynn, S. P. *J. Am. Chem. Soc.* **1976**, *98*, 3815. (f) Peng, S.; Padva, A.; LeBreton, P. R. *Proc. Natl. Acad. Sci. U.S.A.* **1976**, *73*, 2966. (g) Dougherty, D.; McGlynn, S. P. *J. Chem. Phys.* **1977**, *67*, 1289. (h) Yu, C.; Peng, S.; Akiyama, I.; Lin, J.; LeBreton, P. R. *J. Am. Chem. Soc.* **1978**, *100*, 2303. (i) Lin, J.; Yu, C.; Peng, S.; Akiyama, I.; Li, K.; Lee, L.-K.; LeBreton, P. R. *J. Phys. Chem.* **1980**, *84*, 1006. (j) Lin, J.; Yu, C.; Peng, S.; Akiyama, I.; Li, K.; Lee, L.-K.; LeBreton, P. R. *J. Am. Chem. Soc.* **1980**, *102*, 4627.
(16) Kim, H. S.; Yu, M.; Jiang, Q.; LeBreton, P. R. *J. Am. Chem. Soc.* **1993**, *115*, 6169.
(17) Yu, M.; Kim, H. S.; LeBreton, P. R. *Biochem. Biophys. Res. Commun.* **1992**, *184*, 16.
(18) Tasaki, K.; Yang, X.; Urano, S.; Fetzer, S.; LeBreton, P. R. *J. Am. Chem. Soc.* **1990**, *112*, 538.
(19) Kim, H. S.; LeBreton, P. R. *Proc. Natl. Acad. Sci. U.S.A.* **1994**, *91*, 3725.
(20) Vercauteren D. P.; Clementi, E. *Int. J. Quantum Chem., Quantum Biol. Symp.* **1983**, *10*, 11.
(21) (a) Snyder, J. K.; Stock, L. M. *J. Org. Chem.* **1980**, *45*, 1990.
(22) (a) Lawley, P. D.; Thatcher, C. J. *Biochem. J.* **1970**, *116*, 693. (b) Hovinen, J.; Finneman, J. I.; Satapathy, S. N.; Ho, J.; Fishbein, J. C. *J. Am. Chem. Soc.* **1992**, *114*, 10321.
(23) Sieh, D. S.; Michejda, C. J. *J. Am. Chem. Soc.* **1981**, *103*, 442.
(24) Seibel, G. L.; Singh, U. C.; Kollman, P. A. *Proc. Natl. Acad. Sci. U.S.A.* **1985**, *82*, 6537.
(25) York, D. M.; Darden, T.; Deerfield, D.; Pedersen, L. G. *Int. J. Quantum Chem., Quantum Biol. Symp.* **1992**, *19*, 145.
(26) Guldbrand, L. E.; Forester, T. R.; Lynden-Bell, R. M. *Mol. Phys.* **1989**, *67*, 473.
(27) Friedman, H. L. *Chem. Scr.* **1985**, *25*, 42.
(28) (a) Kopka, M. L.; Fratini, A. V.; Drew, H. R.; Dickerson, R. E. *J. Mol. Biol.* **1983**, *163*, 129. (b) Drew, H. R.; Dickerson, R. E. *J. Mol. Biol.* **1981**, *151*, 535.
(29) Westhof, E. *J. Biomol. Struct. Dyn.* **1987**, *5*, 581.
(30) Saenger, W.; Hunter, W. N.; Kennard, O. *Nature* **1986**, *324*, 385.
(31) Falk, M.; Hartman Jr., K. A.; Lord, R. C. *J. Am. Chem. Soc.* **1963**, *85*, 387.
(32) Wolf, B.; Hanlon, S. *Biochemistry* **1975**, *14*, 1661.
(33) Tao, N. J.; Lindsay, S. M. *Biopolymer* **1989**, *28*, 1019.
(34) Falk, M.; Hartman, K. A.; Lord, R. C. *J. Am. Chem. Soc.* **1963**, *85*, 387.
(35) Hearst, J. E.; Vinograd, J. *Proc. Natl. Acad. Sci. U.S.A.* **1961**, *47*, 1005.
(36) Alden, C. G.; Kim, S. H. *J. Mol. Biol.* **1979**, *132*, 411.
(37) Schneider, B.; Cohen, D.; Berman, M. *Biopolymers* **1992**, *32*, 725.

positively identified. However, crystallographic data for dinucleotides which form Watson−Crick base pairs[38] indicate that most Na^+ binding occurs via coordination to the negatively charged O atoms of the phosphate groups. NMR measurements[39] of Na^+ spin relaxation rates in solutions with DNA demonstrate that the binding interaction is primarily electrostatic,[39c,e] and that Na^+ ions bound to DNA undergo rapid exchange with Na^+ ions in bulk solution.[39a,e] The NMR data suggest that, in solutions containing DNA, at a concentration of 100 mg/mL, with 1 equiv of Na^+ and no excess counterions, approximately 90% of the Na^+ lies within 7 Å of the DNA.[39h]

In addition to experimental investigations, descriptions of DNA solvation and of the binding of Na^+ ions to DNA have been obtained from Monte Carlo,[40,41] molecular dynamics,[24,25,42] and diffusion limit Brownian dynamics[26] simulations, and from solutions of the nonlinear Poisson−Boltzmann equation.[43] Molecular dynamics simulations of water coordination and hydrogen-bonding sites on DNA indicate that hydration occurs most favorably on the backbone[42c] at the phosphate groups.[24,42a,b,44] Results from solution of the nonlinear Poisson−Boltzmann equation for the charge density in the environment of DNA,[43] from an approach based on potentials of mean force,[43b] and from Monte Carlo,[40,41,45] diffusion limit Brownian dynamics,[26] and molecular dynamics[24,25,42,44,46] simulations of Na^+ binding to DNA indicate that major binding sites occur in the grooves of DNA and along the backbone at the O atoms of the phosphate groups. Predictions concerning the relative affinity of Na^+ for the grooves versus the backbone vary from one investigation to another, and there is evidence that competition between the two sites depends on temperature[40] and counterion concentration.[43a,47]

Results from earlier theoretical investigations[24−26,40−42,44,46] of Na^+ binding to phosphate groups of DNA have provided differing pictures of the relative importance of binding which occurs via direct coordination of Na^+ to the O atoms of phosphate versus binding which is solvent mediated. Current evidence suggests that both types of binding occur with significant probability. In the clusters examined here, solvent-mediated binding, where water lies between Na^+ and phosphate, has been accounted for.

Electronic Influences on DNA Reactions with Carcinogenic Methylating and Ethylating Agents. In earlier investigations[1,2,14,16,18,19] electronic influences on DNA alkylation patterns observed in reactions with the carcinogenic methylating and ethylating agents, methyl and ethyl methanesulfonate (MeMs and EtMs), dimethyl and diethyl sulfate (Me_2SO_4 and Et_2SO_4), and *N*-methyl-*N*-nitrosourea (MeNU) were considered. With single- and double-stranded DNA and with RNA, reaction at the bases is greatly favored over the reaction at the sugar and phosphate groups.[48] In reactions with the bases, ring nitrogen atoms and exocyclic oxygen atoms are favored sites of attack,[48] and the percentage[48] of the reaction which occurs at the different bases decreases in the order of guanine (62−83) > adenine (7−12) > cytosine (0.7−10) > thymine (0.0−0.8) ≈ uracil (∼0.0). Data for reactions of MeMs, Me_2SO_4, Et_2SO_4, and MeNU with DNA and RNA, which are summarized in Figure 2, indicate that as the first π ionization potential of the nucleotide base decreases the base reactivity increases.[14,16] This comparison provides evidence that electronic factors influence DNA methylation and ethylation patterns. For DNA and RNA, the most reactive site is at N7 of guanine.[48] The apparent correlation between high reactivity and low π ionization potentials is puzzling. For methylation at base heteroatoms by a methane diazonium ion, $CH_3N_2^+$, which is the reactive intermediate in MeNU alkylation of DNA and RNA, computational results[2] from an examination of the transition state, employing the semiempirical MNDO method,[49] indicate that $CH_3N_2^+$ favors an in-plane attack.[2] This suggests that heteroatom lone-pair structure may play an important role in influencing the reactions.

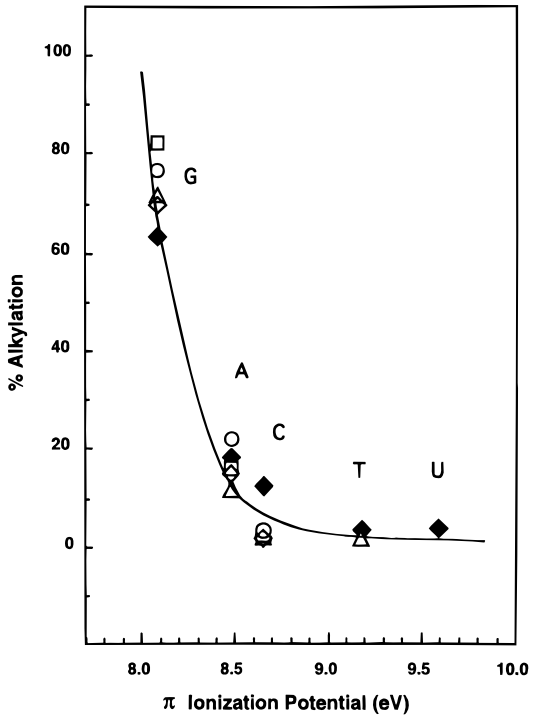

Figure 2. Alkylation patterns for reactions of methyl methanesulfonate (squares), dimethyl sulfate (circles), diethyl sulfate (diamonds), and *N*-methyl-*N*-nitrosourea (triangles). The percentage of total alkylation which occurs at guanine (G), adenine (A), cytosine (C), thymine (T), and uracil (U) is plotted versus experimental base π ionization potentials taken from ref 14. Open symbols show results for double-stranded DNA obtained from reactions with DNA from salmon sperm, calf thymus, salmon testes, rat liver and brain, human fibroblasts, and HeLa and V79 cells. Closed symbols show results for single-stranded DNA and RNA obtained from reactions with DNA from M13 phage, and with RNA from TMV, yeast, HeLa cells, animal ribosomes, and m_2 phage. See ref 48.

(38) (a) Seeman, N. C.; Rosenberg, J. M.; Suddath, F. L.; Kim, J. J. P.; Rich, A. *J. Mol. Biol.* **1976**, *104*, 109. (b) Rosenberg, J. M.; Seeman, N. C.; Day, R. A.; Rich, A. *J. Mol. Biol.* **1976**, *104*, 145.

(39) (a) Anderson, C. F., Record Jr., T. M. *Annu. Rev. Biophys. Biophys. Chem.* **1990**, *19*, 423. (b) Bleam, M. L.; Anderson, C. F., Record, T. M., Jr., *Proc. Natl. Acad. Sci. U.S.A.* **1980**, *77*, 3085. (c) Bleam, M. L.; Anderson, C. F.; Record, T. M., Jr. *Biochemistry* **1983**, *22*, 5418. (d) Nordenskiöld, L.; Chang, D. K.; Anderson, C. F.; Record Jr., T. M. *Biochemistry* **1984**, *23*, 4309. (e) Braunlin, W. H.; Anderson, C. F.; Record, Jr., T. M. *Biopolymers* **1986**, *25*, 205. (f) Anderson, C. F.; Record T. M. Jr.; Hart, P. A. *Biophys. Chem.* **1978**, *7*, 301. (g) Reuben, J.; Shporer, M.; Gabbay, E. J. *Proc. Natl. Acad. Sci. U.S.A.* **1975**, *72*, 245. (h) Strzelecka T. E.; Rill, R. L. *J. Phys. Chem.* **1992**, *96*, 7796. (i) Van Dijk, L.; Gruwel, M. L. H.; Jesse, W.; J. De Bleijser, J.; Leyte, J. C. *Biopolymers* **1987**, *26*, 261.

(40) Clementi, E.; Corongiu, G. *Biopolymers* **1982**, *21*, 763.

(41) Clementi, E. In *Structure and Dynamics: Nucleic Acids and Proteins*; Clementi, E., Sarma, R., Eds.; Adenine Press: New York, 1983; p 321−364.

(42) (a) Forester, T. R.; McDonald, I. R. *Mol. Phys.* **1991**, *72*, 643. (b) Swamy K. N.; Clementi, E. *Biopolymers* **1987**, *26*, 1901. (c) Swaminathan, S.; Ravishanker, G.; Beveridge, D. L. *J. Am. Chem. Soc.* **1991** *113*, 5027.

(43) (a) B. Jayaram, B.; Sharp, K. A.; Honig, B. *Biopolymers* **1989**, *28*, 975. (b) Klein B. J.; Pack, G. R. *Biopolymers* **1983**, *22*, 2331.

(44) Van Gunsteren, W. F.; Berendsen, H. J. C.; Geurtsen, R. G.; Zwinderman, H. R. *J. Anal. N. Y. Acad. Sci.* **1987**, *482*, 287.

(45) Conrad, J.; Troll, M.; Zimm, B. H. *Biopolymers* **1988**, *27*, 1711.

(46) Lee, W. K. Gao, Y.; Prohofsky, E. W. *Biopolymers* **1984**, *23*, 257.

(47) Klement, R.; Soumpasis, D. M.; Jovin, T. M. *Proc. Natl. Acad. Sci. U.S.A.* **1991**, *88*, 4631.

(48) Singer, B.; Grunberger, D. *Molecular Biology of Mutagens and Carcinogens*; Plenum Press: New York, 1983; pp 65−78.

(49) Dewar, M. J. S.; Thiel, W. *J. Am. Chem. Soc.* **1977**, *99*, 4899.

However, a comparison of the percent alkylation which occurs at the different DNA and RNA bases versus PE data indicates that reactivity does not correlate with lone-pair IPs. For example, the lowest energy lone-pair IPs of cytosine, adenine, and guanine are all in the range 9.5−9.7 eV.[14] However, the percent alkylation of guanine, which occurs in reaction with MeNU, is 100 times larger than that of cytosine and 6 times larger than that of adenine.[48]

Other early investigations of electronic influences on DNA methylation patterns have focused on electrostatic potentials and on methyl and ethyl cation affinities.[50−52] The results of MINDO/3 calculations[53] on nucleotide bases[50,51a] indicate that N7 of guanine has the greatest methyl cation affinity, while O^2 of cytosine has the greatest ethyl cation affinity. In contrast with these predictions, a comparison of experimental DNA alkylation patterns for the methylating agents Me_2SO_4 and MeMS versus the ethylating agents Et_2SO_4 and EtMS indicates that in all cases the primary reaction site is N7 of guanine.[48] The results of ab initio SCF calculations with the STO-3G basis set[51b,52] indicate that for the DNA and RNA bases the electrostatic potential is most negative at N7. However, it is reasonable to expect that electrostatic potentials, which are dependent on long-range interactions, will vary significantly with changes in polyanionic DNA and RNA secondary structure. As Figure 2 indicates, the DNA methylation and ethylation patterns for single- and double-stranded DNA are remarkably similar.

In contrast to the view that DNA reactions with $CH_3N_2^+$ are governed most strongly by electrostatic interactions are results from examinations of transition states for gas-phase reactions of $CH_3N_2^+$ and the ethane diazonium ion ($C_2H_5N_2^+$) with nucleotide base model compounds,[1] nucleotide bases, and nucleosides.[2] The results provide evidence that reactions of $CH_3N_2^+$ have greater S_N2 character and a more restricted transition-state volume than reactions of $C_2H_5N_2^+$, which have greater S_N1 character. This examination of the gas-phase transition states has led to the conclusion that $CH_3N_2^+$ reactions have activation barriers which are more strongly influenced by orbital interactions, while $C_2H_5N_2^+$ reactions have barriers which are more strongly influenced by electrostatic interactions. These conclusions are supported by the finding that reaction of $C_2H_5N_2^+$ at the negatively charged phosphate groups of DNA accounts for 57−65% of all DNA modification.[48] For $CH_3N_2^+$, phosphate alkylation accounts for 17% of the DNA modification.

Results from more recent molecular orbital and photoelectron investigations[16,19] suggest that a combination of steric interactions and polarization effects strongly influences DNA alkylation patterns by MeMS, EtMS, Me_2SO_4, Et_2SO_4, and MeNU. Steric factors, for example, the repulsion between the incoming methylating and ethylating agents and the 6-amino group of adenine, cause reaction at N7 of adenine to be significantly less favorable than at N7 of guanine.

Methods

Theoretical IPs of 5′-dGMP$^-$ in clusters containing Na^+ and *n* water molecules where *n* equals 4, 8, 11, 12, and 14 have been obtained by applying Koopmans' theorem[54] to results from ab initio SCF calculations employing the 3-21G basis set[55] and the Gaussian 92 program.[56] Calculations were carried out on a Cray Y/MP4/464 computer, an IBM-SP2/RS6000 cluster with 512 nodes, and a Silicon Graphics/Challenge cluster with 48 processors. The number of water molecules employed in the cluster calculations was restricted by disk space limitations. The 3-21G SCF calculations on cluster **I**, which is shown in Figure 1, required 1.5 Gbytes of disk space on the Cray Y/MP4/464. Molecular orbital diagrams were drawn from molecular orbital coefficients obtained from results of the 3-21G SCF calculations. For 5′-dGMP$^-$ and for the 5′-dGMP$^-\cdot n H_2O\cdot Na^+$ clusters the Gibbs free energies in aqueous solution (ΔG_{ioniz}(solution)) was obtained for the ionization processes

$$(5'\text{-dGMP}^-)_{H_2O} \rightarrow (5'\text{-dGMP}^\bullet)_{H_2O} + e^-$$

and

$$(5'\text{-dGMP}^-\cdot n H_2O\cdot Na^+)_{H_2O} \rightarrow (5'\text{-dGMP}^-\cdot n H_2O\cdot Na^+)^+_{H_2O} + e^-$$

Molecular orbital diagrams in Figures 4−6 and 8 were drawn from molecular orbital coefficients obtained from results of the 3-21G SCF calculations. The inner Gaussian terms of the 3-21G expansions were used for the 2p and 3p orbitals of C, N, O, and P, while the outer Gaussian terms were used for the 2s and 3s orbitals.[16,57] The sizes of the atomic orbitals in the molecular orbital diagrams are proportional to the coefficients. Only atomic orbitals with coefficients greater than 0.15 are shown. In cluster **I** (5′-dGMP$^-\cdot 14H_2O\cdot Na^+$), there are 79 atoms and 330 electrons. The 3-21G SCF wave function contains 717 primitive and 432 contracted basis functions.

Ionization potentials of gas-phase 5′-dGMP$^-$ and of 5′-dGMP$^-$ clusters were obtained using a method in which IPs associated with orbitals localized on the base and sugar groups and on water molecules were obtained by applying Koopmans' theorem to results from 3-21G SCF calculations, and then corrected using HeI UV photoelectron data[16−18,58] from 1,9-dimethylguanine (1,9-Me_2G), 3-hydroxytetrahydrofuran (3-OH-THF), and H_2O.[19] Phosphate group IPs in 5′-dGMP$^-$ and in the 5′-dGMP$^-$ clusters were obtained from 3-21G SCF calculations and were corrected by using theoretical IPs for the model anion $CH_3HPO_4^-$, obtained from post-SCF calculations. These employed second-order Möller−Plesset perturbation (MP2) theory[59] to determine the energies of the ground states of $CH_3HPO_4^-$ and neutral $CH_3HPO_4^\bullet$. The configuration interaction singles (CIS) method[60] was used to determine the energies of the four lowest excited states of $CH_3HPO_4^\bullet$. The MP2 and CIS calculations were carried out with a 6-31+G* basis set.[55,59,61] The first IP of $CH_3HPO_4^-$, obtained from the post-SCF calculations, is equal to the difference between MP2 energies of the ground states of $CH_3HPO_4^-$ and $CH_3HPO_4^\bullet$. The second through fifth IPs were obtained from the CIS excitation energies for $CH_3HPO_4^\bullet$.

Correction of Gas-Phase Ionization Potentials Obtained from SCF Calculations. The method employed for obtaining corrected IPs of 5′-dGMP$^-$ and 5′-dGMP$^-$ clusters, which employs PE data on nucleotide model compounds and post-SCF results on model anions, is the same as the method previously described in the evaluation of ionization potentials of isolated 5′-dCMP$^-$ [18] and 5′-dGMP$^-$ [16,17] and of 5′-dGMP$^-\cdot 4H_2O\cdot Na^+$ clusters.[19] Here, base, sugar, phosphate and

(50) Yu, M. Ph.D. Dissertation, The University of Illinois at Chicago, Chicago, IL, 1992.

(51) (a) Miertus, S.; Trebatickà, M. *Collect. Czech. Chem. Commun.* **1983**, *48*, 3517. (b) Miertus, S.; Trebatickà, M. *J. Theor. Biol.* **1984**, *108*, 509.

(52) Pullman, B. *Ann. N. Y. Acad. Sci.* **1981**, *367*, 182.

(53) Bingham, R. C.; Dewar, M. J. S.; Lo, D. H. *J. Am. Chem. Soc.* **1975**, *97*, 1285.

(54) Koopmans, T. *Physica* **1934**, *1*, 104.

(55) (a) Clark, T.; Chandrasekhar, J.; Spitznagel, G. W.; Schleyer, P. von R. *J. Comput. Chem.* **1983**, *4*, 294. (b) Binkley, J. S.; Pople, J. A.; Hehre, W. J. *J. Am. Chem. Soc.* **1980**. *102*, 939.

(56) Frisch, M. J.; Trucks, G. W.; Head-Gorden, M.; Gill, M. W.; Wong, M. W.; Foresman, J. B.; Johnson, Schlegel, H. B.; Robb, M. A.; Replogle, E. S.; Gomperts, R.; Andres, J. L.; Raghavachari, K.; Binkley, J. S.; Gonzalez, C.; Martin, R. L.; Fox, D. J.; Defrees, D. J.; Baker, J.; Stewart, J. J. P. Pople, J. A. *Gaussian 92*; Gaussian, Inc.: Pittsburgh, PA, 1992.

(57) Clark, T. *A Handbook of Computational Chemistry*; John Wiley: New York, 1985; p 267.

(58) LeBreton, P. R.; Yang, X.; Urano, S.; Fetzer, S.; Yu, M.; Leonard, N. J.; Kumar, S. *J. Am. Chem. Soc.* **1990**, *112*, 2138.

(59) Hehre, W. J.; Radom, L.; Schleyer, P. v. R.; Pople, J. A. *Ab Initio Molecular Orbital Theory*; John Wiley: New York, 1986; pp 38−40, 79, 86.

(60) Foresman, J.; Head-Gordon, M.; Pople, J. A.; Frisch, M. J. *J. Phys. Chem.* **1992**, *96*, 135.

(61) (a) Frisch, M. J.; Pople, J. A.; Binkley, J. S. *J. Chem. Phys.* **1984**, *80*, 3265. (b) The 6-31+G* basis set is the 6-31G* basis set with diffuse functions for non-hydrogen atoms.

water IPs predicted by 3-21G SCF calculations on 5′-dGMP$^-$ and the 5′-dGMP$^-$ clusters, were corrected by employing eqs 1 and 2. These

$$\mathrm{IP}_{\mathrm{corr}}(i) = \mathrm{IP}_{\mathrm{calc}}(i) + \Delta\mathrm{IP}(i) \quad (1)$$

$$\Delta\mathrm{IP}(i) = \mathrm{IP}(i) - \mathrm{IP'}_{\mathrm{calc}}(i) \quad (2)$$

equations rely on the observation that the difference between the corrected IP associated with an occupied orbital in an isolated nucleotide or cluster and the IP obtained from 3-21G SCF calculations is approximately equal to the difference between the corrected IP and the calculated IP associated with the corresponding orbital in 1,9-Me_2G, 3-OH-THF, H_2O, or $CH_3HPO_4^-$.

In eq 1, $IP_{corr}(i)$ is the corrected IP associated with the *i*th orbital in isolated 5′-dGMP$^-$ or in the 5′-dGMP$^-$ cluster, and $IP_{calc}(i)$ is the IP obtained from 3-21G SCF calculations. When eq 2 is used to correct cluster base, sugar, or water IPs, IP(*i*) is the experimental IP associated with the *i*th orbital in 1,9-Me_2G, 3-OH-THF, or H_2O which most closely correlates with the *i*th orbital in the cluster. $IP'_{calc}(i)$ is the IP of the *i*th orbital in 1,9-Me_2G, 3-OH-THF, or H_2O obtained from 3-21G SCF results. When eq 2 is used to correct IPs of the anionic phosphate group, IP(*i*) is the IP calculated at the post-SCF level.

Evaluation of Gibbs Free Energies of Hydration. Gibbs free energies of hydration, ΔG_{hyd}, were calculated for 5′-dGMP$^-$ and 5′-dGMP$^-$ clusters before and after ionization by employing a Langevin dipole relaxation method[62] and the Polaris 3.2 program.[62b−d] For calculations of ΔG_{hyd}, the atomic charges of 5′-dGMP$^-$ and of the 5′-dGMP$^-$ clusters before and after ionization were needed. For calculations of ΔG_{hyd} before ionization, atomic charges were obtained from 3-21G SCF results for the ground states of 5′-dGMP$^-$ and of the 5′-dGMP$^-$ clusters. The atomic charges used to calculate values of ΔG_{hyd} after ionization of the base, sugar, or phosphate groups of 5′-dGMP$^-$ and of 5′-dGMP$^-$ clusters were obtained by modifying the 3-21G atomic charges of the closed-shell ground-state nucleotide. For ionization of the base, the modified atomic charges were obtained by subtracting the charge of a single electron distributed over the base atoms of 5′-dGMP$^-$ and of 5′-dGMP$^-$ clusters. The distribution of the removed electron was obtained by subtracting the 3-21G SCF atomic charge distribution for the ground state of the radical cation (5′-dGMP$^-$·$4H_2O$·Na^+)$^+$ from that of the ground state of 5′-dGMP$^-$·nH_2O·Na^+, in which the highest occupied molecular orbital (HOMO) is a π orbital residing on the base. For ionization of the sugar, the modified atomic charges were obtained by subtracting the charge of an electron distributed over the sugar atoms of 5′-dGMP$^-$ and of 5′-dGMP$^-$ clusters. The distribution of the removed electron was obtained by subtracting the 3-21G SCF atomic charge distribution for the ground state of the radical cation 3-OH-THF$^+$ from that of the ground state of 3-OH-THF. For ionization of the phosphate group in 5′-dGMP$^-$ and 5′-dGMP$^-$ clusters, the distribution of the removed electron was obtained by subtracting the 3-21G SCF atomic charge distribution for the ground state of the radical 5′-dGMP•, in which the HOMO is an O atom lone-pair orbital on the phosphate group, from that of the ground state of 5′-dGMP$^-$.

In calculations of ΔG_{ioniz}(solution), the solvation energy of the electron was not included because in many chemically significant events involving the removal of electrons from DNA the electrons are not solvated in the final state but donated to an electron acceptor. For example, in electrochemical reactions, electrons are donated to an anode. In electrophilic attack of DNA, electrons are shared with an electrophile.

Determination of Free Energies of Ionization in Solution. The Gibbs free energies of ionization in aqueous solution (ΔG_{ioniz}(solution)) were obtained by employing the gas-phase IPs and the differences ($\Delta\Delta G_{hyd}$) between the Gibbs free energies of hydration for isolated 5′-dGMP$^-$ or 5′-dGMP$^-$ clusters before and after ionization. Here, ΔG_{ioniz}(solution) is given by eq 3, where ΔG_{ioniz}(gas) is the free energy of ionization in the gas phase, and $\Delta\Delta G_{hyd}$ is given by eq 4. In eq 4, $\Delta G_{hyd}(1)$ and $\Delta G_{hyd}(2)$ are the free energies of hydration before and after ionization, respectively. The rationale for eq 3 is provided by the thermodynamic cycle shown in Figure 3. In eq 5, ΔH_{ioniz}(gas) is

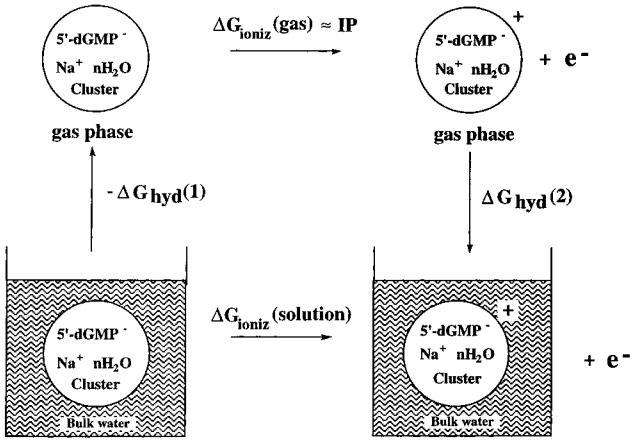

Figure 3. Thermodynamic cycle from which the solution free energies of ionization (ΔG_{ioniz}(solution)) of 5′-dGMP$^-$ in clusters and of 5′-dGMP$^-$ not incorporated into clusters were obtained. Values of ΔG_{ioniz}(solution) are given by eqs 3−5, where ΔG_{ioniz}(gas) is obtained from corrected gas-phase IPs.

$$\Delta G_{\mathrm{ioniz}}(\mathrm{solution}) = \Delta G_{\mathrm{ioniz}}(\mathrm{gas}) + \Delta\Delta G_{\mathrm{hyd}} \quad (3)$$

$$\Delta\Delta G_{\mathrm{hyd}} = \Delta G_{\mathrm{hyd}}(2) - \Delta G_{\mathrm{hyd}}(1) \quad (4)$$

$$\Delta G_{\mathrm{ioniz}}(\mathrm{gas}) = \Delta H_{\mathrm{ioniz}}(\mathrm{gas}) - T\Delta S_{\mathrm{ioniz}}(\mathrm{gas}) \approx \mathrm{IP} \quad (5)$$

the corrected gas-phase ionization potential of 5′-dGMP$^-$ or of a 5′-dGMP$^-$ cluster and ΔS_{ioniz}(gas) is the change in entropy associated with ionization of 5′-dGMP$^-$ or of 5′-dGMP$^-$ clusters in the gas phase. Compared to ΔH_{ioniz}(gas), $T\Delta S_{ioniz}$(gas) is negligible, so that ΔG_{ioniz}(gas) ≈ ΔH_{ioniz}(gas). This approximation is supported by the observation that, by electron convention Fermi−Dirac statistics, $T\Delta S$ for the ionization of a hydrogen atom at room temperature is 0.05 eV.[63] It is also supported by results of 3-21G SCF calculations indicating that at room temperature $T\Delta S$ for the lowest energy gas-phase ionization of 3-OH-THF is less than 0.1 eV.

Geometries. A planar ring geometry was used for calculations on 1,9-dimethylguanine. Heavy atom bond lengths and bond angles, H atom bond angles, and torsional angles describing CH_3 rotation were optimized at the 3-21G SCF level. The N−H bond length was 1.01 Å, and the C−H bond lengths were 1.10 and 1.08 Å.[64] The geometry used for calculations on 3-hydroxytetrahydrofuran was obtained by combining electron diffraction data for tetrahydrofuran[65] with standard OH bond lengths and bond angles. The C−O bond length in the hydroxyl group was 1.43 Å, the CCO bond angle was 111.4°, and the OCCO dihedral angle was −86.1°.

For calculations on the model anion $CH_3HPO_4^-$, a geometry based on X-ray data was employed. The geometry of $CH_3HPO_4^-$ was taken by combining the phosphate group heavy atom bond lengths and bond angles in (deoxycytidylyl)-(3′−5′)-deoxyguanosine[66] with H−O−P−O and the C−O−P−O dihedral angles which were set equal to the C−O−P−O dihedral angles obtained from optimized X-ray data for B-DNA.[67] The O−H and C−H bond lengths were 0.95 and 1.1 Å, respectively. Two of the HCO bond angles were 108.8°; one was 110.7°. The HOP bond angle was 107.6°. The H−C−O−P dihedral angle, describing rotation of the CH_3 group around the C−O bond, was 146°. The nucleotide geometry, used in calculations of 5′-dGMP$^-$ in cluster **I**, of

(62) (a) Atkins; P. W. *Physical Chemistry*, 5th ed.; W. H. Freeman and Co.: New York, 1994; p 758. (b) Warshel, A.; Russell, S. T. *Q. Rev. Biophys.* **1984**, *17*, 288. (c) Lee, F. S.; Chu. Z. T.; Warshel, A. *J. Comput. Chem.* **1993**, *14*, 161. (d) Russell, S. T.; Warshel, A. *J. Mol. Biol.* **1985**, *185*, 389. (e) Warshel, A. *Proc. Natl. Acad. Sci. U.S.A.* **1978**, *75*, 5250. (f) Warshel, A.; Åqvist, J *Annu. Rev. Biophys. Biophys. Chem.* **1991**, *20*, 267. (g) Warshel, A.; Levitt, M. *J. Mol. Biol.* **1976**, *103*, 227.

(63) Bartmess, J. E. *J. Phys. Chem.* **1994**, *98*, 6420.

(64) Bowen, H. J. M.; Donohue, J.; Jenkin, D. G.; Kennard, O.; Wheatley, P. J.; Whiffen, D. H. In *Tables of Interatomic Distances and Configuration in Molecules and Ions;* Sutton, L. E., Jenkin, D. G., Mitchell, A. D., Cross, L. C., Eds.; The Chemical Society: London, 1958; pp M67, S7, S15−S17.

(65) Geise, H. J.; Adams, W. J.; Bartell, L. S. *Tetrahedron* **1969**, *25*, 3045.

(66) Cruse, B. T.; Egert, E.; Kennard, O.; Sala, G. B.; Salisbury, S. A.; Visamitra, M. A. *Biochemistry* **1983**, *22*, 1833.

(67) Arnott, S.; Hukins, W. L. *Biochem. Biophys. Res. Commun.* **1972**, *47*, 1504.

Table 1. A Comparison of Experimental and Calculated Ionization Potentials for the Model Compounds 1,9-Dimethylguanine (1,9-Me_2G), 3-Hydroxytetrahydrofuran (3-OH-THF), and H_2O and for the Model Anion $CH_3HPO_4^-$ [a]

				SCF			
				6-31G		3-21G	
molecule or anion	orbital	orbital type	IP[b]	IP_{calc}	$\Delta IP(j)^f$	IP_{calc}	$\Delta IP(j)^f$
1,9-Me_2G	B_1	π	8.09[c]	8.00	−0.09	7.83	−0.26
	B_2	π	9.5−10.0[c]	10.36	0.4−0.9	10.21	0.2−0.7
	B_3	n	9.5−10.0[c]	11.14	1.1−1.6	10.88	0.9−1.4
	B_4	π	9.5−10.0[c]	11.21	1.2−1.7	11.03	1.0−1.5
	B_5	n	9.5−10.0[c]	11.67	1.7−2.2	11.47	1.5−2.0
	B_6	π	11.0[c]	12.05	1.1	11.93	0.9
	B_7	n	11.0[c]	12.71	1.7	12.45	1.5
3-OH-THF	S_1	n	9.77[d]	11.21	1.44	10.96	1.19
	S_2	n	10.66[d]	12.14	1.48	11.82	1.16
H_2O	W_1	n	12.62[e]	13.64	1.02	12.99	0.37
$CH_3HPO_4^-$	P_1	n	4.69	6.00	1.31	4.87	0.18
	P_2	n	5.90	6.37	0.47	5.19	-0.71
	P_3	n	6.20	7.18	0.98	6.12	-0.08
	P_4	n	6.83	7.12	0.29	6.25	-0.58
	P_5	n	8.63	8.28	−0.35	7.36	-1.27

[a] All ionization potentials in electronvolts. [b] Ionization potentials of molecules obtained from experiment. Ionization potentials of anions obtained from post-SCF calculations using the MP2/CIS method. See ref 19. [c] Obtained from ref 58. [d] Obtained from ref 16. [e] Obtained from ref 71. [f] Obtained via eq 2.

other clusters, and of isolated 5′-dGMP$^-$, is the same as that described previously.[16,19] For water molecules, the H−O−H bond angle is 105°.[64]

In cluster **I**, the water−counterion interactions with 5′-dGMP$^-$, are favorable, and most or all of these interactions are expected to occur dynamically when DNA is in an aqueous environment containing counterions. The geometry of the cluster was chosen by combining X-ray data with results from geometry optimization calculations on components of the cluster. Water molecules labeled 1−8 and 13 in Figure 1 (W(1) to W(8) and W(13)) make up part of an inner solvation shell. Molecules W(9) to W(11) and W(14) make up part of a second shell. Water molecules W(2) to W(7) were restricted to an octahedral symmetry around Na^+.

Molecules W(1), W(8), W(12), and W(14) were restricted to geometries which are coplanar with the guanine group, and molecules W(2) to W(5) and W(9) to W(11) were fixed in geometries which are coplanar with Na^+ and the P and negatively charged O atoms of the phosphate group. The O atoms of W(1), W(8), and W(13) are located 3.00, 3.50, and 3.68 Å from the heteroatoms N3, O^6, and O5″, respectively. The positions of these water molecules were chosen on the basis of X-ray data for water molecules interacting with B-DNA oligonucleotides.[29] N7 is another position at which X-ray data indicate there is strong interaction with H_2O. In cluster **I**, the distance chosen (4.50 Å) between W(12) and N7 is consistent with the X-ray data,[29] indicating that tight binding does not occur simultaneously at N7 and O^6.

The distance (2.4 Å) between Na^+ and the O atoms of the octahedrally symmetric water molecules (W(2) to W(7)) was obtained via a separate SCF optimization of the isolated cluster with a 6-31G basis set.[68,69] The distance (2.87 Å) between the O atoms of W(9) to W(11) and the closest O atoms of the inner shell water molecules (W(2), W(3), and W(5)) was obtained from a separate 3-21G SCF optimization calculation on Na^+, W(2) to W(7), and W(9) to W(11). In this calculation, Na^+ and W(2) to W(7) were fixed in the 6-31G SCF optimized octahedral geometry, Na^+, W(2),W(3),W(5), and W(9) to W(11) were restricted to a local C_{2v} symmetry, and the O atoms of W(2), W(3), W(9), and W(11) were held colinear. The distance between Na^+ and the negative O atoms of the phosphate group (5.00 Å) was obtained from a 6-31G SCF optimization calculation[19] in which a component of cluster **I**, containing Na^+ and W(2) to W(4), was docked to the component containing 5′-dGMP$^-$ and W(1). Here the two individual components had fixed geometries which were the same as those in cluster **I**.

In calculations on clusters containing 5′-dGMP$^-$ and Na^+ with 4, 8, 11, and 12 water molecules, the geometries were based on that of cluster **I**. The geometries of 5′-dGMP$^-$ and Na^+ are the same as in cluster **I**. In the clusters containing 4, 8, 11, and 12 water molecules the geometries of the water molecules are the same as water molecules W(1) to W(4), W(1) to W(8), W(1) to W(11), and W(1) to W(12) in cluster **I**.

For a calculation on 2′-deoxyribose 5′-phosphate, the geometry was the same as that of the deoxyribose and the phosphate groups in 5′-dGMP$^-$. In calculations on two guanine·$CH_3HPO_4^-$ supermolecules, the geometries were based on that of 5′-dGMP$^-$. The rotational orientation of guanine and $CH_3HPO_4^-$ in the supermolecules was the same as that of the guanine and phosphate groups in 5′-dGMP$^-$. In one of the supermolecules, the distance between the N9 atom of guanine and the P atom of $CH_3HPO_4^-$ was 5.01 Å. The geometry of the second guanine·$CH_3HPO_4^-$ supermolecule was obtained from the translation of the $CH_3HPO_4^-$ anion along the line of the N9−C1′ bond in 5′-dGMP$^-$ to a position where the distance between the N9 and P atoms was 10.45 Å.

Results

Table 1 compares experimental vertical IPs of 1,9-Me_2G, 3-OH-THF, and water with theoretical IPs obtained by applying Koopmans' theorem to results from SCF calculations with the 6-31G and 3-21G basis sets. The table also compares IPs of the model anion $CH_3HPO_4^-$, obtained from 6-31G and 3-21G SCF calculations with IPs from post-SCF calculations[16,19] using the combined MP2/CIS methods.

For all the neutral molecules and $CH_3HPO_4^-$, the 6-31G SCF ionization potentials are larger than those from 3-21G SCF calculations. For 3-OH-THF and H_2O, the IPs of O atom lone-pair orbitals obtained from both 6-31G and 3-21G SCF calculations are larger than experimental vertical IPs. The 6-31G and 3-21G SCF values of the lowest IP of 1,9-Me_2G, which is associated with a π orbital (B_1), are both smaller than the experimental value. All other IPs of 1,9-Me_2G obtained from 6-31G and 3-21G SCF calculations are larger than the experimental values. The lowest π ionization potential from the 6-31G SCF calculations (8.00 eV) agrees with the experimental vertical IP (8.09 eV) better than the value (7.83 eV) obtained from 3-21G SCF calculations. The lowest energy lone-pair IP of 1,9-Me_2G, obtained from the 6-31G SCF calculations (11.14 eV) is more than 1 eV larger than the experimental IP (9.5−10.0 eV). Similar results were obtained for the lowest energy oxygen atom lone-pair IPs in 3-OH-THF and H_2O. Here, the lowest experimental vertical IPs (9.77 and 12.62 eV, respectively) are 1.44 and 1.02 eV smaller than the 6-31G SCF values. For 1,9-Me_2G, 3-OH-THF, and H_2O, the lowest lone-

(68) (a) Hehre, W. J.; Ditchfield, R.; Pople, J. A. *J. Chem. Phys.* **1972**, *56*, 2257. (b) P. C. Hariharan, Pople, J. A. *Theor. Chim. Acta* **1973**, *28*, 213.

(69) Gordon, M. S. *Chem. Phys. Lett.* **1980**, *76*, 163.

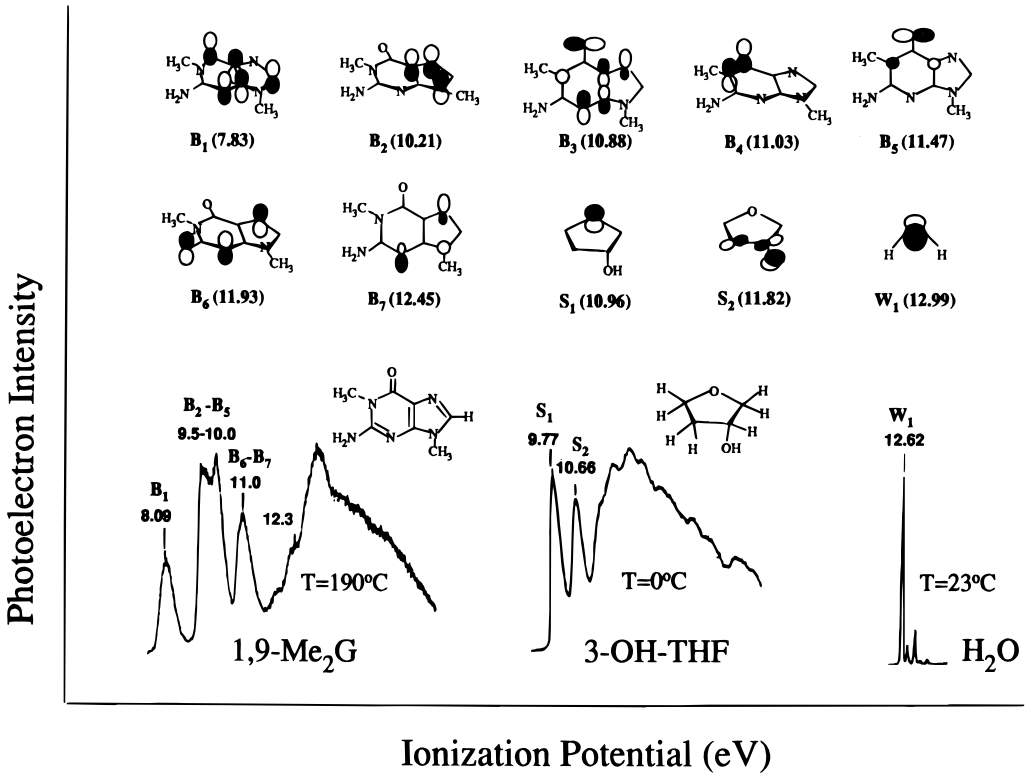

Figure 4. Photoelectron spectra and assignments for 1,9-dimethylguanine (1,9-Me_2G), 3-hydroxytetrahydrofuran (3-OH-THF), and water, taken from refs 16, 58, and 71. Theoretical ionization potentials and orbital diagrams obtained from 3-21G SCF calculations are also given.

pair IPs obtained from 3-21G SCF calculations agree better with experiment than the 6-31G SCF values; however, they are still 0.9−1.4, 1.19, and 0.37 eV larger than the experimental vertical IPs.

For $CH_3HPO_4^-$, the five lowest IPs are associated with oxygen atom, lone-pair orbitals. Earlier investigations[16,18] provided evidence that the first IP of $CH_3HPO_4^-$ obtained from MP2 calculations (4.69 eV) is accurate to ±0.4 eV. The first IP of $CH_3HPO_4^-$ obtained from 6-31G SCF calculations (6.00 eV) is significantly larger than that from the MP2 calculations; however, the value obtained from 3-21G SCF calculations (4.87 eV) is in good agreement. Preliminary results[70] from calculations on $CH_3HPO_4^-$ using the multireference CI method with singles and doubles and a complete active space SCF wave function suggest that values of the second through fourth IPs of $CH_3HPO_4^-$, which were obtained from the MP2/CIS method are 0.5−0.8 eV too large. Because of the high excitation associated with the fifth IP, the error in the MP2/CIS prediction of this value is expected to be even greater.

Figure 4 shows HeI UV photoelectron spectra with assignments,[16,58,71] and orbital diagrams obtained from 3-21G SCF calculations on 1,9-Me_2G, 3-OH-THF, and H_2O. The orbital diagrams in Figure 4 agree well with previously reported diagrams obtained from 6-31G SCF calculations.[16,19] Earlier investigations[72,73] employed HAM/3 CI calculations[74,75] to test the qualitative validity of a Koopmans' theorem description of low-energy ionization events in 1,9-Me_2G and 3-OH-THF. The HAM/3 CI results indicate that the electron hole distribution in cation states giving rise to the S_1 and S_2 bands of 3-OH-THF and the B_1, B_3, B_5, B_6, and B_7 bands of 1,9-Me_2G are qualitatively well described by Koopmans' theorem. The HAM/3 CI calculations also indicate that hole-mixing contributes to ionization events associated with the B_2 and B_4 orbitals of 1,9-Me_2G. Here, the IPs of the hole mixing states are predicted to lie in a poorly resolved region of the PE spectrum between 9.5 and 10.0 eV.[16,58] This is the energy region assigned to the B_2 and B_4 bands in Figure 4.

To test descriptions of electron holes associated with ionization of $CH_3HPO_4^-$, results from closed-shell 3-21G SCF calculations on $CH_3HPO_4^-$ were compared to results from ab initio MP2/CIS calculations on the neutral radical $CH_3HPO_4^{\bullet}$. Figure 5 shows orbital diagrams (P_1 to P_5) for the five highest occupied orbitals in $CH_3HPO_4^-$ obtained from 3-21G SCF calculations. The figure also contains orbital representations of electron holes in $CH_3HPO_4^{\bullet}$. These are labeled P_1' to P_5' and are associated with the five lowest energy ionization events in $CH_3HPO_4^-$ as predicted by MP2/CIS calculations. The procedure used to determine the distribution in the electron hole representations has been described previously.[16]

The similarity between the wave functions described by P_1 and P_1' provides evidence that Koopmans' theorem yields a qualitatively valid description of the lowest energy ionization of $CH_3HPO_4^-$. This conclusion is supported by examination of the lowest unoccupied molecular orbital (LUMO) in the lowest energy configuration of the ground-state MP2 wave function of $CH_3HPO_4^{\bullet}$. The LUMO hole distribution in $CH_3HPO_4^{\bullet}$ is similar to that of the occupied P_1 orbital of $CH_3HPO_4^-$, as described by 3-21G SCF calculations. In the MP2 ground-state wave function of CH_3HPO_4, the coefficient of the lowest energy configuration is 1.0. The coefficients of configurations other than the lowest energy configuration are all less than 0.1.

Representations P_2' to P_5' were obtained from results of CIS calculations. The right side of Figure 5 represents holes appearing in the major configurations contributing to the excited

(70) Fetzer, S.; Rohmer, M.-M.; Veillard, A. Private communication.
(71) Kimura, K.; Katsumata, S.; Achiba, Y.; Yamazaki, T.; Iwata, S. *Handbook of HeI Photoelectron Spectra of Fundamental Organic Molecules*; Halsted: New York, 1981; p 33.
(72) Yu, M.; Jiang, Q.; LeBreton, P. R. *Int. J. Quantum Chem., Quantum Biol. Symp.* **1992**, *19*, 27.
(73) Jiang, Q. Ph.D. Dissertation, The University of Illinois at Chicago, Chicago, IL, 1994.
(74) Lindholm, E.; Asbrink, L. *Molecular Orbitals and their Energies, Studied by the Semiempirical HAM Method*; Springer-Verlag: New York, 1985.
(75) Chong, D. P. *J. Mol. Sci.* **1982**, *2*, 55.

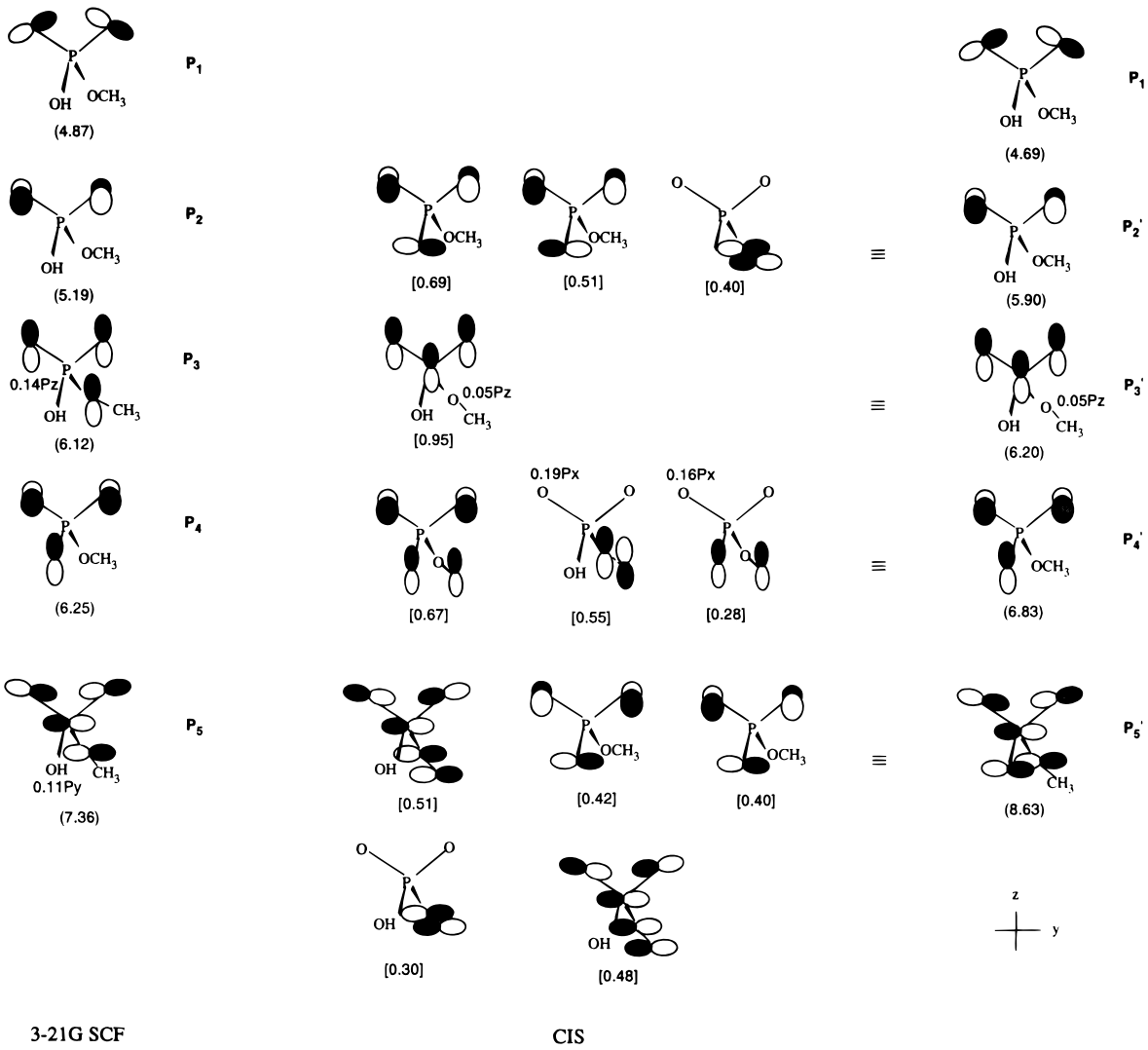

Figure 5. Diagrams for the five highest occupied orbitals (P_1 to P_5) of $CH_3HPO_4^-$ obtained from 3-21G SCF calculations (shown on the left), and electron holes (P_1' to P_5') associated with the five lowest energy ionization events in $CH_3HPO_4^-$ (shown on the right) obtained from results of 6-31+G* MP2 and CIS calculations on $CH_3HPO_4^-$ and $CH_3HPO_4^{\bullet}$. Ionization potentials, eV, are given in parentheses. The electron hole P_1' was drawn by comparing results from MP2 calculations on the ground states of $CH_3HPO_4^-$ and $CH_3HPO_4^{\bullet}$. Electron holes P_2' to P_5' were drawn by comparing results from CIS calculations, describing the excited states of $CH_3HPO_4^{\bullet}$ with results from 3-21G SCF calculations on $CH_3HPO_4^-$. Diagrams of P_2' to P_5' were drawn by using atomic orbital coefficients associated with 6-31+G* molecular orbitals occupied in $CH_3HPO_4^-$, but unoccupied in configurations which significantly contribute to the CI wave functions describing the states of $CH_3HPO_4^{\bullet}$ examined. The 6-31+G* orbitals are shown in the center. Atomic orbital coefficients employed in the electron hole diagrams were obtained by multiplying the molecular orbital coefficients by the configuration coefficients, given in brackets. It should be noted that the P_1' to P_5' composite electron holes provide an orbital representation of ionization events which are described by post-SCF wave functions. In this regard, they are not rigorous.

states of $CH_3HPO_4^{\bullet}$. Results from CIS calculations indicate that the composite holes, P_2' through P_5', associated with the second through fifth lowest energy ionization events in $CH_3HPO_4^-$, are similar to holes in 3-21G SCF Koopmans' configurations, associated with removal of electrons from the P_2 through P_5 orbitals. The only major difference is that P_3' has significant contribution from the phosphorus $3P_z$ atomic orbital which is absent in the 3-21G SCF description of the P_3 orbital of $CH_3HPO_4^-$.

Corrected Ionization Potentials without Solvent Polarization. Figure 6 contains corrected IPs and orbital diagrams associated with the 14 highest occupied orbitals in 5′-dGMP$^-$, and with the 28 highest occupied orbitals in cluster **I**. Of the 28 highest occupied orbitals in the cluster, 14 are located on 5′-dGMP$^-$ and 14 on water molecules. Like previously reported 6-31G SCF results for isolated 5′-dGMP$^-$ and for 5′-dGMP$^-$·-4H_2O·Na^+ clusters,[16,19] the upper occupied nucleotide orbitals described by 3-21G SCF calculations on 5′-dGMP$^-$ and cluster **I** are largely localized on either the base, sugar, or phosphate groups. In Figure 6, these are labeled B, S, and P, respectively. Furthermore, the nucleotide orbitals have electron distributions like those of corresponding orbitals in 1,9-Me_2G, 3-OH-THF, and $CH_3HPO_4^-$, which are shown in Figures 4 and 5. Of the 14 highest occupied nucleotide orbitals in cluster **I**, only one is significantly delocalized on more than one group. This orbital, labeled B_2', is a mixture of the B_2 orbital in 1,9-Me_2G and the P_4 orbital in $CH_3HPO_4^-$.

In Figure 6, the value of $\Delta IP(j)$ employed in eq 1 to obtain the corrected ionization potential ($IP_{corr}(j)$) associated with the B_2' orbital was taken to be the same (0.2−0.7 eV) as that used to obtain the corrected IPs associated with the B_2 orbital in isolated 5′-dGMP$^-$. Support for this method of correcting B_2' ionization in cluster **I** is provided by a comparison of 3-21G SCF results for cluster **I** with results for the 5′-dGMP$^-$·8H_2O·Na^+ cluster. The results indicate that the cluster with eight H_2O molecules contains a localized B_2 orbital. Furthermore, the 3-21G SCF energy of the B_2 orbital in 5′-dGMP$^-$·8H_2O·Na^+ differs from that of the B_2' orbital in cluster **I** by only 0.2 eV.

In Figure 6, the corrected phosphate IPs of isolated 5′-dGMP$^-$ and of 5′-dGMP$^-$ in cluster **I** were obtained by using a

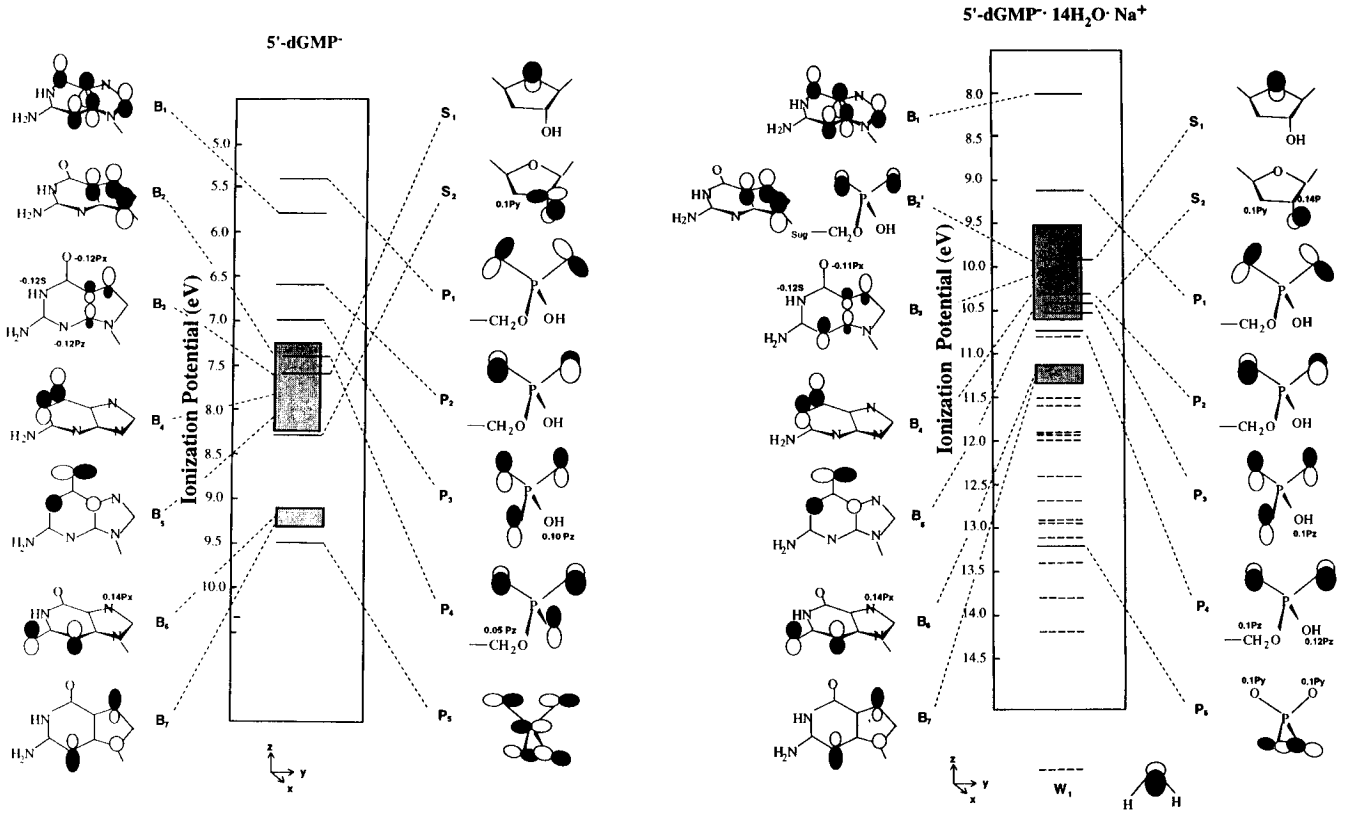

Figure 6. Corrected ionization potentials and orbital diagrams for the 14 highest occupied orbitals in 5′-dGMP$^-$ and for the 28 highest occupied orbitals including 14 water orbitals in 5′-dGMP$^-$·14H_2O·Na^+ (cluster **I**). The orbitals localized on the base, sugar, and phosphate groups and on the water molecules are designated B, S, P, and W, respectively. For 5′-dGMP$^-$ all of the orbitals are localized. For cluster **I**, only one of the nucleotide orbitals, B_2', which resides on both the base and phosphate groups, is significantly delocalized. The B_2' orbital is formed from a mixing of orbitals similar to the B_2 orbital in 1,9-Me_2G and the P_4 orbital in $CH_3HPO_4^-$. The hatched area corresponds to an energy region containing orbitals in 1,9-Me_2G, which give rise to unresolved PE bands. For all molecular orbitals, only atomic orbitals with coefficients greater than 0.15 are shown. In some cases, values of coefficients less than 0.15 are given.

Table 2. Phosphate Ionization Potentials Obtained from 3-21G SCF Calculations[a]

	guanine·$CH_3HPO_4^-$ [b]	2′-deoxyribose 5′-phosphate	5′-dGMP$^-$
P_1	4.99 (5.26)	5.31	5.60
P_2	5.29 (5.56)	5.62	5.91
P_3	6.21 (6.47)	6.53	6.81
P_4	6.30 (6.60)	6.62	6.94
P_5	7.56 (7.87)	7.86	8.23

[a] Ionization potentials obtained via application of Koopmans' theorem and given in electronvolts. [b] Ionization potentials obtained when the distance between N9 and P was 10.45 Å are given without parentheses. Ionization potentials obtained when the distance was 5.01 Å are given in parentheses.

procedure which is different from that employed earlier.[16,18] In earlier work (see eq 7 of ref 1), corrected phosphate IPs of 5′-dCMP$^-$ and 5′-dGMP$^-$ were taken to be equal to corresponding IPs in $CH_3HPO_4^-$.[16,18] The procedure used here, which employs eqs 1 and 2, accounts for differences between the perturbing effects of the sugar and base groups in 5′-dGMP$^-$ versus the methyl group in $CH_3HPO_4^-$. Table 2 lists IPs from 3-21G SCF calculations on two supermolecules containing guanine and $CH_3HPO_4^-$ (guanine·$CH_3HPO_4^-$). In the supermolecules, the distances between N9 of guanine and the P atom of $CH_3HPO_4^-$ were 5.01 and 10.45 Å. The former distance is the same as that which occurs in 5′-dGMP$^-$ in B-DNA. Table 2 also contains phosphate IPs obtained from 3-21G SCF calculations on 2′-deoxyribose 5′-phosphate and on 5′-dGMP$^-$.

According to the results in Table 2, the phosphate IPs in the guanine·$CH_3HPO_4^-$ supermolecule, where the distance between N9 and P is 5.01 Å, are 0.35 to 0.51 eV larger than corresponding IPs of isolated $CH_3HPO_4^-$, which are listed in Table 1. The phosphate IPs in guanine·$CH_3HPO_4^-$, where the distance between N9 and P is 10.45 Å, are 0.05 to 0.20 eV larger than corresponding IPs in $CH_3HPO_4^-$. Table 2 demonstrates that changing from a methyl to a 2′-deoxyribosyl group also influences the phosphate IPs. In 2′-deoxyribose 5′-phosphate the 3-21G SCF calculations predict that the P_1 to P_5 ionization potentials are 0.37−0.50 eV larger than corresponding IPs in isolated $CH_3HPO_4^-$. The combination of perturbations associated with the through-space interaction with guanine and the deoxyribosly ester linkage gives rise to phosphate IPs in 5′-dGMP$^-$ which are 0.7−0.9 eV larger than corresponding IPs in $CH_3HPO_4^-$. Finally, in considering the phosphate IPs in Figure 6, it is important to note that the results in Figure 4 provide evidence that the electron hole describing P_3 ionization in 5′-dGMP$^-$, which is based on Koopmans' theorem, must be modified to reflect the effects of configuration interaction.

A comparison of the corrected IPs in Figure 6 for isolated 5′-dGMP$^-$ versus 5′-dGMP$^-$ in cluster **I** indicates that electrostatic stabilization by Na^+ in the cluster increases all of the nucleotide IPs. For the lowest energy base, sugar, and phosphate orbitals, the corrected IPs of the cluster are 2.1, 2.3, and 3.7 eV larger than corresponding IPs in isolated 5′-dGMP$^-$. In the cluster, the binding of Na^+ to the phosphate group causes an increase of phosphate IPs which is greater than that of the base or sugar IPs, and results in a change in the ordering. For isolated 5′-dGMP$^-$, the IP of the phosphate group is 0.4 eV smaller than that of the base. For cluster **I**, the IP of the base is 1.1 eV smaller than that of the phosphate group.

The top panel of Figure 7 compares the corrected lowest IPs of the base, sugar, and phosphate groups in isolated 5′-dGMP$^-$ with corresponding IPs in cluster **I**. The figure demonstrates

Table 3. Hydration Energies (ΔG_{hyd}) and the Differences ($\Delta\Delta G_{hyd}$) between Hydration Energies of the Neutral Clusters 5′-dGMP$^-$·nH_2O·Na^+ and of Cations Obtained by Removal of an Electron from the Clusters[a]

	ΔG_{hyd}				$\Delta\Delta G_{hyd}$		
	before	after ionization					
n	ionization	B[b]	S[c]	P[d]	B	S	P
4	−62.66	−88.85	−95.40	−87.45	−26.19	−32.74	−24.19
8	−62.31	−88.69	−94.20	−85.05	−26.38	−31.89	−22.74
11	−70.60	−92.85	−98.16	−86.88	−22.25	−27.56	−16.06
12	−70.07	−94.72	−97.99	−86.26	−24.65	−27.92	−16.19
14	−65.74	−96.78	−98.05	−85.63	−29.24	−30.51	−18.09
5′-dGMP$^-$	−83.07[e]	−64.97[f]	−65.75[f]	−37.04[f]	18.10	17.32	46.03

[a] Energies are given in kilocalories per mole. [b] Electron distribution associated with the lowest energy base ionization. [c] Electron distribution associated with the lowest energy sugar ionization. [d] Electron distribution associated with the lowest energy phosphate ionization. [e] 5′-dGMP$^-$ anion. [f] 5′-dGMP neutral radical.

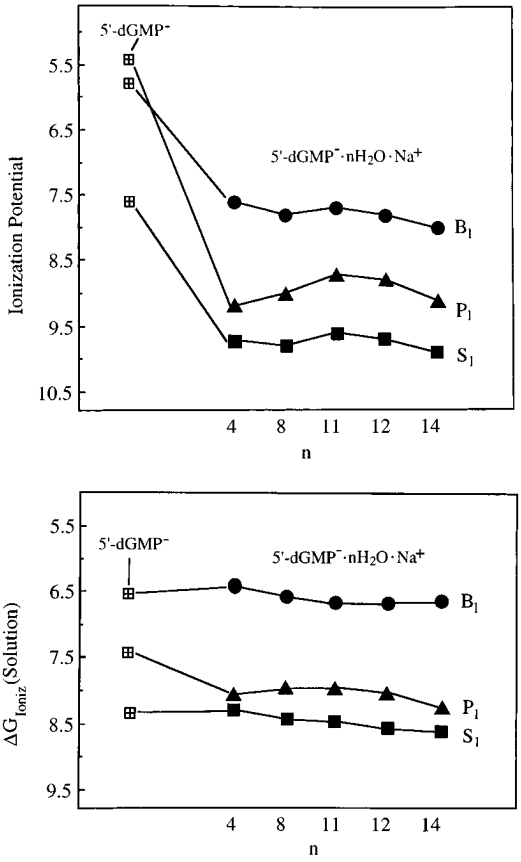

Figure 7. (Upper panel) Lowest energy corrected IPs of the base, sugar, and phosphate groups of 5′-dGMP$^-$, and of 5′-dGMP$^-$·nH_2O·Na^+ clusters containing 4, 8, 11, 12, and 14 water molecules. (Lower panel) Gibbs free energy of ionization in solution (ΔG_{ionz}(solution)) for the lowest energy ionization events associated with the base, sugar, and phosphate groups in 5′-dGMP$^-$ and in 5′-dGMP$^-$·nH_2O·Na^+ clusters. Ionization potentials and values of ΔG_{ionz}(solution) are given in electronvolts.

that Na^+ electrostatic stabilization is the dominant factor causing differences between the IPs of isolated 5′-dGMP$^-$ compared to 5′-dGMP$^-$ in clusters. The results indicate that the corrected lowest base, sugar, and phosphate IPs for clusters containing 5′-dGMP$^-$ with Na^+ and 4, 8, 11, and 12 water molecules are larger than in isolated 5′-dGMP$^-$ by 1.8−2.0, 2.0−2.2, and 3.3−3.8 eV, respectively. They also demonstrate that direct interactions with H_2O have a much smaller effect on 5′-dGMP$^-$ ionization potentials than does electrostatic stabilization by Na^+. For cluster **I**, with 14 water molecules, the lowest base, sugar, and phosphate IPs differ by no more than 0.4, 0.1, and 0.2 eV from corresponding IPs in 5′-dGMP$^-$·4H_2O·Na^+. The conclusion that Na^+ electrostatic effects are important to the increase in IPs associated with the gas-phase clusters versus isolated 5′-dGMP$^-$ is supported by a supplementary calculation of a cluster containing only 5′-dGMP$^-$ and Na^+, in which the nucleotide−counterion geometry is the same as that in cluster **I**. Here, the increases in the lowest energy, corrected, base, sugar, and phosphate IPs compared to those of isolated 5′-dGMP$^-$ represent more than 63% of the corresponding increases found when the IPs of cluster **I** and isolated 5′-dGMP$^-$ are compared.

Gibbs Free Energies of Ionization in Solution. In the present investigation, theoretical Gibbs free energies of hydration (ΔG_{hyd}) for the monovalent cations Na^+, NH_4^+, $N(CH_3)H_3^+$, $N(C_2H_5)H_3^+$, and $N(CH_3)_3H^+$ obtained from Langevin dipole relaxation calculations using Polaris 3.2 were found to differ from experimental free energies by 0.02−0.31 eV. Similar results were reported previously.[62c] Table 3 lists values of ΔG_{hyd} for the clusters 5′-dGMP$^-$·nH_2O·Na^+ where *n* equals 4, 8, 11, 12, and 14 and for 5′-dGMP$^-$ not incorporated in a cluster. Values of ΔG_{hyd} are given before and after ionization. The values of ΔG_{hyd}, calculated after ionization, have been obtained for the lowest energy base (B), sugar (S), and phosphate (P) ionization events. The results indicate that, before and after ionization, there are significant differences between values of ΔG_{hyd} calculated for the clusters and for 5′-dGMP$^-$ not incorporated in a cluster. These differences arise because hydration energies of ions are greater than those of neutral clusters or radicals. Before ionization, the largest value of ΔG_{hyd} is for 5′-dGMP$^-$ not incorporated in a cluster. After ionization, values of ΔG_{hyd} are smallest for 5′-dGMP· neutral radicals, which are not incorporated in a cluster. For clusters containing different numbers of water molecules (4−14), the differences between corresponding values of ΔG_{hyd}, either before or after ionization, are not large. Before ionization, the differences between the ΔG_{hyd} values of the different clusters are less than 5.7 kcal/mol. After base, sugar, or phosphate ionization, the differences between the ΔG_{hyd} values are less than 8.1, 3.9, or 1.8 kcal/mol, respectively. The small changes in ΔG_{hyd} for clusters containing varying numbers of water molecules provide evidence that large contributions to ΔG_{hyd} are associated with relaxation outside the first solvation shell of the 5′-dGMP$^-$·-Na^+ ion pair.

Table 3 also compares differences ($\Delta\Delta G_{hyd}$) between free energies of hydration before and after ionization for clusters and for 5′-dGMP$^-$ not incorporated in a cluster. Like values of ΔG_{hyd}, values of $\Delta\Delta G_{hyd}$ do not change greatly as the cluster size increases from 4 to 14 water molecules. For the lowest energy base, sugar, and phosphate ionization events, the differences between the $\Delta\Delta G_{hyd}$ values of the five different clusters are less than 7.0, 5.2, and 8.1 kcal/mol, respectively. The sign of $\Delta\Delta G_{hyd}$ for the neutral clusters is opposite that of 5′-dGMP$^-$ not incorporated in a cluster.

For cluster **I** and for 5′-dGMP$^-$ in aqueous solution, Figure 8 shows the Gibbs free energies of ionization (ΔG_{ioniz}(solution)) associated with the 14 highest occupied orbitals. The lower

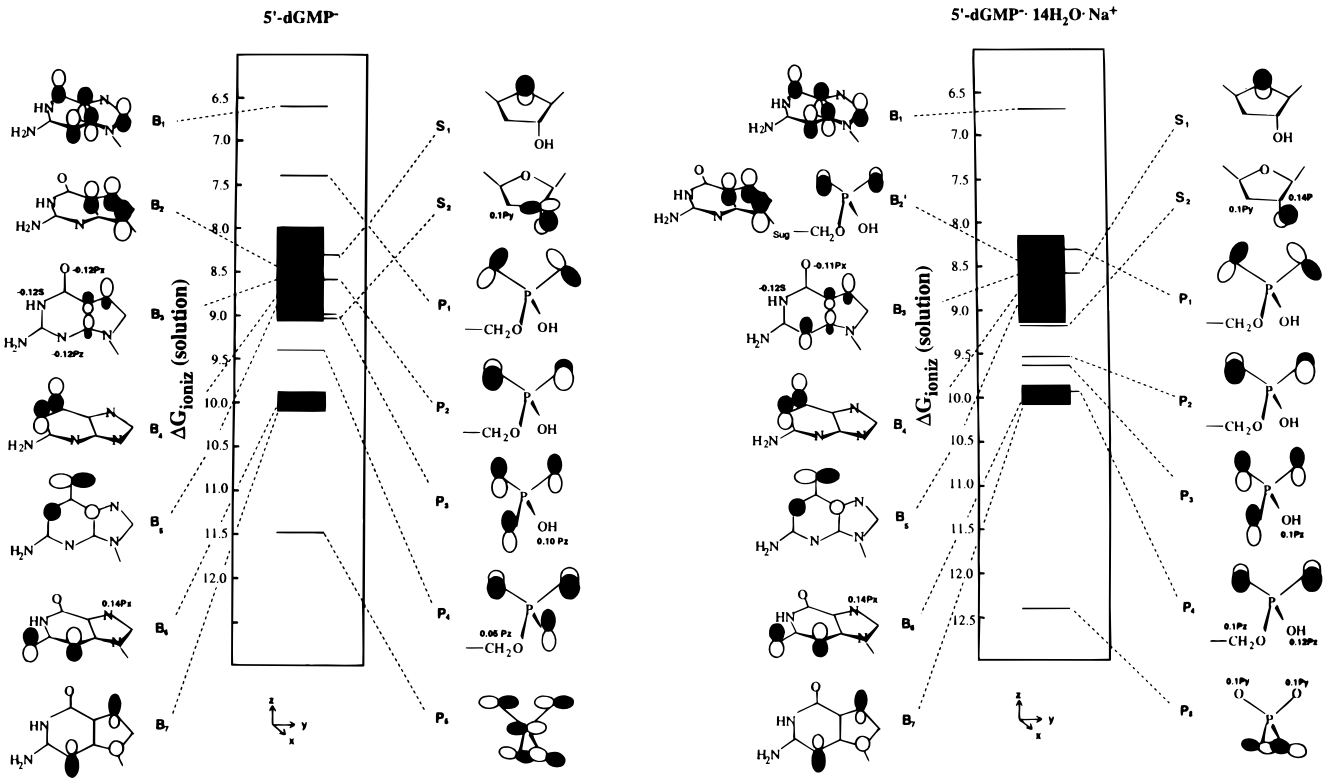

Figure 8. Free energies of ionization in solution (ΔG_{ionz}(solution) for 5′-dGMP$^-$ and for 5′-dGMP$^-$·14H_2O^+·Na^+ (cluster **I**). Orbital diagrams are the same as those given in Figure 5. As in Figure 5 the hatched area corresponds to an energy region containing orbitals in 1,9-Me_2G, which give rise to unresolved PE bands.

panel of Figure 7 contains values of ΔG_{ioniz}(solution) for the lowest energy base, sugar, and phosphate ionization events in 5′-dGMP$^-$ not incorporated in a cluster and in the clusters 5′-dGMP$^-$·*n*H_2O·Na^+ for *n* equal to 4, 8, 11, 12, and 14. A comparison of results in Figure 6 and in the top panel of Figure 7 with the results in the bottom panel of Figure 7 and in Figure 8 indicates that hydration effects reduce the ionization energies of the base, sugar, and phosphate groups in cluster **I**, but increase the ionization energies in 5′-dGMP$^-$ not incorporated in a cluster. For cluster **I**, the absolute values of the differences between ΔG_{ioniz}(gas) and ΔG_{ioniz}(solution) for the lowest energy base, sugar, and phosphate ionization events are 1.27, 1.32, and 0.78 eV, respectively. For 5′-dGMP$^-$, the corresponding differences are 0.78, 0.75, and 2.00 eV.

The lower panel of Figure 7 provides evidence that values of ΔG_{ioniz}(solution) do not vary greatly as the number of water molecules in the clusters changes. For the lowest energy base, sugar, and phosphate ionization events, the differences between the values of ΔG_{ioniz}(solution) for the different clusters are less than 0.3, 0.4, and 0.3 eV, respectively. The relatively small changes in ΔG_{ioniz}(solution) for clusters of varying size reflect the finding that the values of $\Delta\Delta G_{hyd}$ do not vary greatly when the number of water molecules in the cluster changes from 4 to 14. The results in the upper and lower panels of Figure 7 indicate further that differences between corresponding values of ΔG_{ioniz}(solution) for the clusters versus 5′-dGMP$^-$ not incorporated in a cluster are much smaller than the differences between the gas-phase IPs. Finally, the finding, in Figure 7, that values of ΔG_{ioniz}(solution) for 5′-dGMP$^-$ with or without a cluster are smaller for base ionization than for sugar or phosphate ionization is consistent with ESR data indicating that, in an aqueous environment at 77 K and neutral pH, γ-irradiated 5′-dGMP$^-$ gives rise to highly stable radicals in which guanine is positively charged.[76]

(76) Gregoli, S.; Olast, M.; Bertinchamps, A. *Radiat. Res.* **1977**, *72*, 201.

Discussion

Results from 3-21G SCF calculations on cluster **I** indicate that nucleotide valence orbitals are generally localized on the base, sugar, or phosphate groups, and that electronic distributions in these orbitals are similar to those in corresponding orbitals of 1,9-Me_2G, 3-OH-THF, and $CH_3HPO_4^-$. The electrostatic stabilization by Na^+ results in gas-phase base, sugar, and phosphate IPs in cluster **I** which are more than 2 eV larger than in isolated 5′-dGMP$^-$, and which are ordered differently. In cluster **I**, the gas-phase IP of the base is 1.1 eV smaller than that of the phosphate group. In 5′-dGMP$^-$, the IP of the phosphate group is 0.4 eV smaller than that of the base. In gas-phase clusters, the effects of water on the IPs of 5′-dGMP$^-$ are small. When clusters containing 4, 8, 11, 12, and 14 H_2O molecules are compared, the corresponding lowest energy base, sugar, and phosphate IPs differ by less than 0.5 eV.

Because the procedure for obtaining corrected gas-phase IPs (eqs 1 and 2) employs the same level of theory for the model compounds and anions, and for the nucleotide and nucleotide clusters, different computational methods yield similar IPs. At the 6-31G SCF level, the corrected lowest energy IPs of the base, sugar, and phosphate groups in 5′-dGMP$^-$ are 5.9, 7.8, and 5.4 eV, respectively.[19] At the 3-21G SCF level, the corrected IPs are 5.8, 7.6, and 5.4 eV. Similarly, the corresponding corrected IPs obtained from 6-31G SCF calculations[19] on 5′-dGMP$^-$·4H_2O·Na^+ (7.7, 10.0, and 9.0 eV) agree well with corrected IPs from 3-21G SCF calculations (7.6, 9.7, and 9.2 eV). However, different methods yield uncorrected IPs, obtained directly from Koopmans' theorem, which are significantly different. The uncorrected lowest energy phosphate IP obtained from 6-31G SCF calculations on 5′-dGMP$^-$ [16,19] is 1.1 eV larger than that obtained from 3-21G SCF calculations. The observation that the corrected IPs are not strongly basis set dependent provides evidence that the correction procedure employed here

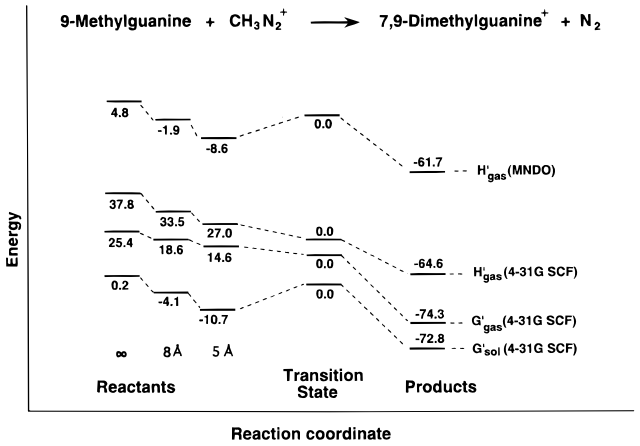

Figure 9. Differences between Gibbs free energies (G') and enthalpies (H') for reactants, reactant ion−molecule complexes, and products, referenced to an approximate transition-state geometry obtained from MNDO calculations on the gas-phase N7 methylation of 9-methylguanine by $CH_3N_2^+$. Values of G' and H' are in kilocalories per mole. Results are from 4-31G SCF and MNDO calculations. Values of H' are given for the gas-phase reaction. Values of G' are given for the reaction in the gas phase and in water. For reaction in water, the Gibbs free energy referenced to the transition state was calculated using eq 6.

will yield similar values for IPs obtained not only from ab initio calculations but also from a variety of semiempirical SCF calculations.

Table 3 indicates that differences between Gibbs free energies of hydration, before and after ionization ($\Delta\Delta G_{hyd}$), contribute significantly to free energies associated with ionization in aqueous solution (ΔG_{ioniz}(solution)). In all of the clusters, hydration has the effect of reducing ΔG_{ioniz}(solution). The effect of hydration on the ionization energies of 5′-dGMP$^-$, which is not incorporated into a cluster, is similar in magnitude, but opposite in sign, to the effect of hydration on the ionization energies of the clusters. As indicated in Figure 7, the opposing influence that hydration has on ΔG_{ioniz}(solution) for 5′-dGMP$^-$ not incorporated in clusters versus 5′-dGMP$^-$ in clusters causes corresponding values of ΔG_{ioniz}(solution) for the two nucleotide systems to be similar. A comparison of 5′-dGMP$^-$ not incorporated in a cluster versus 5′-dGMP$^-$ in cluster **I** indicates that differences between the corresponding lowest energy gas-phase IPs of the base, sugar, and phosphate groups are 2.2, 2.3, and 3.7 eV, respectively. In contrast, differences between values of ΔG_{ioniz}(solution) are 0.1, 0.3, and 0.9 eV. The smaller differences between values of ΔG_{ioniz}(solution) provide evidence that, for clusters in solution, the increase in IPs, associated with Na^+ electrostatic stabilization, is nearly canceled by differences ($\Delta\Delta G_{hyd}$) between the Gibbs free energies of hydration before and after ionization. This suggests that ΔG_{ioniz}(solution) remains relatively constant in solutions of varying ionic strength.

Hydration Effects on Activation Barriers for Nucleotide−Methane diazonium Ion Reactions. Earlier investigations of reactions of MeNU with nucleotides focused on an S_N2 mechanism in which methanediazonium ions ($CH_3N_2^+$) are reactive intermediates.[1,2,16,77] The selectivity of $CH_3N_2^+$ in nucleotide methylation reactions provides evidence that activation barriers exist.[48] Figure 9 summarizes results from gas-phase MNDO calculations of the enthalpy at various stages in the gas-phase reaction of $CH_3N_2^+$ with N7 of the nucleoside model compound 9-methylguanine (9-MeG). Enthalpy differences (H'_{gas}) referenced to the transition state were calculated for the separated reactants and products (cationic 7,9-dimethylguanine plus N_2), and for reactant ion−molecule complexes. Geometries were obtained using AMPAC, employing MNDO and a nonlinear, least-squares gradient minimization procedure.[78,79] For the reactants, products, and transition state, full optimization calculations were carried out.[80] In calculations on the reactant ion−molecule complexes, the distances between the carbon atom (C′) of the methanediazonium ion and N7 of 9-MeG were 8 and 5 Å.[81]

The results in Figure 9 indicate that, for the complexes, the enthalpies are lower than that of the separated reactants. These results provide evidence of a potential minimum and of an intrinsic barrier similar to that described in previous investigations of gas-phase, ion−molecule methyl transfer reactions.[82] Figure 9 also shows results from ab initio SCF calculations with a 4-31G basis set[83] which are different from the MNDO results. For the gas-phase reaction, the enthapies from the ab initio calculations provide no evidence of a barrier. The ab initio results predict that the enthalpy and Gibbs free energy referenced to the transition state (G'_{gas}) decrease monotonically as reaction proceeds. One explanation of the ab initio results is that the reaction potential surface is significantly influenced by hydration effects. In aqueous solution, specific rates for S_N2 methyl transfer reactions are, in some cases, 20 orders of magnitude slower than in the gas phase.[84] Furthermore, for ion−molecule nucleophilic displacement reactions in hydrated clusters, reaction barrier heights increase as the number of water molecules increases.[85,86]

Ab initio 4-31G SCF results summarized in Figure 9 provide evidence that the reaction barrier depends on hydration. Here, an examination of the barrier, in aqueous solution, for reaction of $CH_3N_2^+$ at N7 of 9-MeG was carried out by calculating the change in the Gibbs free energy of the system in solution (G'_{sol}) at various points on the reaction surface relative to the transition state. Values of G'_{sol} were obtained calculating differences between the Gibbs free energies in solution (G_{sol}), obtained from eq 6, at different points on the reaction surface. Here, G_{gas} is

$$G_{sol} = G_{gas} + \Delta G_{hyd} \qquad (6)$$

the gas-phase Gibbs free energy of the system obtained from 4-31G SCF calculations. For the 4-31G SCF calculation on the transition state, the geometry obtained from MNDO calculations on the gas-phase reaction was used.[87] In eq 6, ΔG_{hyd} is the hydration energy of the system calculated using Polaris 3.2. For the reactant ion−molecule complexes, ΔG_{hyd} was taken to be approximately equal to the hydration energy of the separated reactants.

(77) (a) Lawley P. D. In *Chemical Carcinogenesis;* Searle, C. E., Ed.; ACS Monograph 182; American Chemical Society: Washington, DC, 1984; pp 325−484. (b) Hathway, D. E.; Kolar, G. F. *Chem. Soc. Rev.* **1980**, *9*, 241.

(78) Dewar, M. J. S.; Thiel, W. *J. Am. Chem. Soc.* **1977**, *99*, 4899.

(79) Liotard, D. A.; Healy, E. F.; Ruiz, J. M.; Dewar, M. J. S. *AMPAC 2.2*; QCPE 506: Indiana University.

(80) For the transition-state geometry, a vibrational frequency calculation yielded one imaginary frequency.

(81) In these complexes, 9-MeG and $CH_3N_2^+$ were in the separated reactant geometries and N_2 of $CH_3N_2^+$ was directed away from N7. For the complex in which the C′−N7 distance was 8 Å, the C′ and nitrogen atoms of $CH_3N_2^+$ were coplanar with the ring atoms of 9-MeG and the N′−C′−N7 angle was fixed at 180°. The potential was not strongly dependent on the C′−N7−C8 angle. The value used (127.8°) corresponded to a local AMPAC minimum. For the complex in which the C′−N7 distance was 5 Å, the N′−C′−N7 and the C′−N7−C8 angles were also 180° and 127.8°.

(82) (a) Pellerite, M. J.; Brauman, J. I. *J. Am. Chem. Soc.* **1983**, *105*, 2672. (b) Pellerite, M. J.; Brauman, J. I. *J. Am. Chem. Soc.* **1980**, *102*, 5993.

(83) (a) Ditchfield, R.; Hehre, W. J.; Pople, J. A. *J. Chem. Phys.* **1971**, *54*, 724. (b) Hehre, W. J.; A. Lathan, W. A. *J. Chem. Phys.* **1972**, *56*, 5255.

(84) Tanaka, K.; Mackay, G. I.; Payzant, J. D.; Bohme, D. K. *Can. J. Chem.* **1976**, *54*, 1643.

(85) Bohme, D. K.; Mackay, G. I. *J. Am. Chem. Soc.* **1981**, *103*, 978.

(86) Morokuma, K. *J. Am. Chem. Soc.* **1982**, *104*, 3732.

Table 4. Calculated Energies for Reactions of Methanediazonium Ions with Nucleoside Model Compounds

nucleoside model compound	methylation site	ΔH_{gas}[a–c] MNDO[f]	ΔH_{gas}[a–c] 4−31G[k]	$\Delta H^{\ddagger}_{gas}$[b–f]	$\Delta G^{\ddagger}_{sol}$[b,g]	r_{form}[e,f,h,i]	r_{break}[e,f,h,j]
9-methylguanine	N7	−66.4 (−62.9)	−103.6	−2.5 (−2.0) [9.8]	4.1	2.192	1.828
	N3	−45.0 (−45.0)	−70.0	17.6 (15.8)	23.6	2.263	1.899
	O^6	−61.5 (−58.6)	−81.9	1.4 (1.0)	4.7	2.438	2.145
9-methyladenine	N7	−57.5 (−54.6)	−84.2	5.0 (7.0)	21.8	2.186	1.823
	N1	−58.3 (−56.7)	−93.0	6.2 (7.8)	10.5	2.205	1.875
	N3	−59.4 (−61.3)	−89.4	8.5 (7.1)	12.7	2.229	1.806
1-methylcytosine	O^2	−69.1 (−67.0)	−92.8	−1.7 (−1.8) [11.0]	4.9	2.159	1.891
	N3	−58.2 (−56.3)	−99.9	0.9 (3.4)	7.4	2.347	1.976
1-methylthymine	O^4	−48.2 (−45.6)	−58.	5.0 (8.5)	6.3	2.418	2.232
	O^2	−46.3 (−45.0)	−53.9	7.0 (9.8)	8.9	2.415	2.219

[a] Enthalpy of reaction. In all cases, the reaction products are dimethylated nucleotide base cations and N_2. For reaction at N7 of 9-methylguanine, the geometries used for calculations on the reactants and products are described in the text. For all other reactions, the geometries were obtained using the same method. [b] In kilocalories per mole. [c] After correction for zero point energy. [d] Values without parentheses are differences between gas-phase enthalpies of the transition states and of the reactant monomethyl nucleoside model compounds plus $CH_3N_2^+$. Values in parentheses are enthalpy differences, taken from ref 2, for reactions in which guanine, adenine, cytosine, and thymine were the reactants. For reaction at N7 of 9-methylguanine and at O^2 of 1-methylcytosine, values in brackets are gas-phase enthalpy differences between the transition states and reactant ion−molecule complexes, in which the distance between the C′ atom and the reactive atom of the base was 5 Å. See the text. For all reactions, the transition state geometries were determined using the procedure described in the text for reaction at N7 of 9-methylguanine. [e] Obtained from MNDO calculations. [f] Results in parentheses were obtained for reactions in which unmethylated guanine, adenine, cytosine, and thymine were reactants. These results were taken from ref 2. [g] Approximate Gibbs free energy barrier heights for reactions of nucleoside model compounds in aqueous solution. Values given are differences between Gibbs free energies of solvated reactant ion−molecule complexes, in which the distance between the C′ atom of $CH_3N_2^+$ and the reactive atom of the base was 8 Å, and of solvated transition states. Free energy differences between the gas-phase reactant ion−molecule complexes and the transition state were obtained from ab initio 4−31G SCF calculations. Geometries used in the ab initio calculations, and the procedure used to calculate the differences between the free energies of solvation between the reactant ion−molecule complexes and the transition states are described in the text and in ref 90. [h] In angstroms. [i] Length of the breaking bond in the transition state. [j] Length of the forming bond in the transition state. [k] Calculated using AMPAC-optimized geometries for reactants and products. See the text.

Values of G'_{sol} given in Figure 9 indicate that, in the transition state, the Gibbs free energy exhibits a barrier, and is 10.7 kcal/mol larger than that for the ion−molecule complex in which the C′−N7 distance is 5 Å. The occurrence of the barrier depends on the larger hydration energy (−71.68 kcal/mol) of the small, charged reactant $CH_3N_2^+$ compared to the hydration energy (−56.81 kcal/mol) of the transition state.[88]

Table 4 compares gas-phase enthalpies of reaction (ΔH_{gas}) obtained from 4-31G SCF and MNDO calculations. The 4-31G SCF values, obtained from AMPAC geometries, are 14−42% larger than the MNDO values. The table also lists MNDO values of the difference ($\Delta H^{\ddagger}_{gas}$) between the gas-phase enthalpies of the transition states and those of the separated reactants, and calculated lengths of the breaking and forming bonds (r_{break} and r_{form}) in the transition states. For reaction at N7 of 9-MeG and at O^2 of 1-methylcytosine (1-MeC), where the MNDO results indicate that the transition-state enthalpy is lower than that of the reactants, the occurrence of intrinsic barriers is indicated by values of $\Delta H^{\ddagger}_{gas}$ given in brackets. These values are the differences between the gas-phase, transition-state enthalpies and the enthalpies of reactant ion−molecule complexes in which the distance between the C′ atom and the reactive atom of the base was 5 Å.[89]

The method, employed in Figure 9 to examine G'_{sol} for reaction at N7 of 9-MeG, was also used to examine reactions at N3 and O^6 of 9-MeG, at N1, N3, and N7 of 9-methyladenine (9-MeA), at O^2 and N3 of 1−MeC, and at O^2 and O^4 of 1-methylthymine (1-MeT). Table 4 lists values of $\Delta G^{\ddagger}_{sol}$, which are equal to the difference between the Gibbs free energies in solution of the transition states and the free energies of partially optimized reactant ion−molecule complexes in which the distance between C′ and a selected heteroatom of the base was 8 Å.[90] Values of $\Delta G^{\ddagger}_{sol}$ were obtained using eq 6. In evaluation of $\Delta G^{\ddagger}_{sol}$, the transition-state geometries were again obtained from MNDO calculations on the gas-phase reactions. Like the reaction of $CH_3N_2^+$ at N7 of 9-MeG in aqueous solution, the other reactions all exhibit barriers, with values of $\Delta G^{\ddagger}_{sol}$ greater than zero. Values of $\Delta G^{\ddagger}_{sol}$ listed in Table 4 are only approximations of activation barrier heights in solution. However, with the exception of the reaction at N7 of 9-MeA,[91] the ordering of $\Delta G^{\ddagger}_{sol}$ values, obtained from ab initio calculations, is similar to the ordering of $\Delta H^{\ddagger}_{gas}$ values, obtained from MNDO

(87) Although the ab initio calculations indicate that hydration is critical to the occurrence of the reaction barrier, geometries used in single-point ab initio 4-31G SCF calculations, for reaction of $CH_3N_2^+$ at N7 of 9-methylguanine, and for reactions with other nucleoside model compounds, were obtained from gas-phase MNDO transition-state calculations. This compromise was made because accurate descriptions of the transition states for reactions of these large systems in solution are not currently available, and because rough features of the transition-state geometries in solution are likely to be similar to the gas-phase geometries obtained from the MNDO calculations.

(88) The calculated value of ΔG_{hyd} for the neutral reactant 9-methylguanine was −9.53 kcal/mol.

(89) For the ion−molecule complex associated with reaction at N7 of 9-MeG, the geometry was the same as that used to obtain the results in Figure 9. For the complex associated with reaction at O^2 of 1-MeC, the base and $CH_3N_2^+$ were in the separated reactant geometries, N_2 of $CH_3N_2^+$ was directed away from O^2, the heavy atoms of $CH_3N_2^+$ were coplanar with the heavy atoms of 1-MeC, and the N′−C′−O^2 angle was fixed at 180°. The C′−O^2−C2 angle (134.2°) corresponded to a local AMPAC minimum.

(90) Because of the approximate nature of these calculations, the energy of only one complex was computed for all of the reactions of each nucleoside model compound. In all reactant complex geometries, the heavy atoms of $CH_3N_2^+$ and of the nucleoside models were in the same plane, and $CH_3N_2^+$ and the nucleoside models were in the separated reactant geometries. For reactions at N7, N3, and O^6 of 9-MeG, the geometry of the complex used to calculate $\Delta G^{\ddagger}_{sol}$ was the same as that used to obtain the results in Figure 9. In the complex used for calculations of $\Delta G^{\ddagger}_{sol}$ for reactions at O^2 and N3 of 1-MeC, the C′−N3 distance was 8 Å, the N′−C′−N3 angle was fixed at 180°, and the C′−N3−C2 angle was 48.1°. In the complex used for calculations on reactions at N1, N3, and N7 of 9-MeA, the C′−N7 distance was 8 Å, the N′−C′−N7 angle was fixed at 180°, and the C′−N7−C8 angle was 127.6°. In the complex used for calculations on reactions at O^2 and O^4 of 1-MeT, the C′−O^2 distance was 8 Å, the N′−C′−O^2 angle was fixed at 180°, and the C′−O^2−C4 angle was 126.5°. The C′−N3−C2, C′−N7−C8, and C′−O^2−N3 angles in the 1-MeC, 9-MeA, and 1-MeT complexes corresponded to local AMPAC minima.

(91) For 9-MeA, the value of $\Delta G^{\ddagger}_{sol}$ corresponding to reaction at N7 is 9−12 kcal/mol greater than values for reaction at N1 or N3. In contrast, values of $\Delta H^{\ddagger}_{gas}$ for reactions at N1, N3, and N7 differ by less than 3 kcal/mol. Polaris 3.2 calculations, indicating that the Gibbs free energy of hydration of the transition state for reaction at N7 is 5−6 kcal/mol smaller than hydration energies of transition states for reactions at N1 and N3, suggest that the large value of $\Delta G^{\ddagger}_{sol}$ for reaction at N7 is due in part to solvation effects.

Table 5. Differences between Base Heavy Atom π Orbital, Gross Electron Populations of Reactants and Those of Transition States for Reactions of Nucleoside Models with Methanediazonium Ions

base	methylation site	$\Delta q_{\pi\ \mathrm{total}}$ (eu) HF/4−31G	HF/6-31G	MNDO
9-methylguanine	N7	0.496	0.499	0.540
	N3	0.431	0.447	0.475
	O^6	0.410	0.433	0.474
9-methyladenine	N7	0.824	0.832	0.806
	N1	0.406	0.412	0.450
	N3	0.383	0.392	0.467
1-methylcytosine	O^2	0.391	0.396	0.458
	N3	0.385	0.392	0.447
1-methylthymine	O^4	0.448	0.446	0.490
	O^2	0.341	0.373	0.439

calculations on the gas-phase reactions. Both $\Delta G^{\ddagger}_{sol}$ and $\Delta H^{\ddagger}_{gas}$ values are largest for reaction at N3 of 9-MeG, and both values are smallest for reaction at N7 of 9-MeG,[92] which experiment indicates is most favorable.

π Polarization and Steric Influences on DNA Methylation and Ethylation Patterns. The high reactivity at N7 of guanine in S_N2 methylation and ethylation reactions and the increase in base reactivity which occurs as base π ionization potentials decrease have led to speculation[16,19] that π perturbation in nucleotides influences base reactivity. Earlier investigations[93] provided evidence that π polarization influences base−base and base−ligand stacking interactions, and that polarizabilities increase as π ionization potentials decrease.[93b,c] Association constants for stacked base complexes, like the reactivities shown in Figure 2, increase as π ionization potentials decrease.[93b,c]

To examine the relationship between reactivity and π polarizability, the change in base heavy atom π electron population ($\Delta q_{\pi\ \mathrm{total}}$) which occurs as the reaction proceeds from reactants to the transition state has been evaluated using eq 7.

$$\Delta q_{\pi\ \mathrm{total}} = \sum |\Delta e_{\pi}(i)| \qquad (7)$$

In eq 7, $|\Delta e_{\pi}(i)|$ is the absolute value of the difference between the π electron population on heavy atom *i* in the isolated base versus the transition state. Table 5 lists values of $\Delta q_{\pi\ \mathrm{total}}$ obtained from MNDO calculations, and from ab initio 4-31G and 6-31G SCF calculations, employing MNDO transition-state geometries.

Results from both the ab initio and the MNDO calculations, indicating that sites on the purines, specifically N7 of 9-MeA and 9-MeG, have the largest values of $\Delta q_{\pi\ \mathrm{total}}$, agree with Figure 2 which demonstrates that purines are more reactive than pyrimidines. However, the larger value of $\Delta q_{\pi\ \mathrm{total}}$ for N7 of 9-MeA compared to N7 of 9-MeG does not agree with the higher reactivity at N7 of guanine. An explanation of this apparent inconsistency is provided by considering the transition state for reaction of $CH_3N_2^+$ at N7 of 2′-deoxyadenosine,[16] in which there is steric crowding between the methyl group of $CH_3N_2^+$ and the exocyclic amino group at C6 of the base. This causes rotation of the amino group out of the plane of the base, resulting in unfavorable perturbation of the π system. Consistent with the hypothesis that π polarization is important in determining base reactivity, the results in Table 5 indicate that, for transition states in which the base remains planar, the largest value of $\Delta q_{\pi\ \mathrm{total}}$ occurs for reaction at N7 of 9-MeG.

Conclusions

In summary the main results obtained from this investigation are the following.

(1) The localized orbital structure of nucleotides makes it possible to employ PE data and results from post-SCF calculations on model compounds and anions to correct nucleotide valence IPs obtained from SCF calculations. With this method, the 14 lowest energy base, sugar, and phosphate IPs of 5′-dGMP$^-$ and of a 5′-dGMP$^-$ cluster containing 14 H_2O molecules and an Na^+ ion bound to phosphate have been evaluated. When combined with Gibbs free energies of hydration, this approach also provides Gibbs free energies ($\Delta G_{\mathrm{ioniz}}$(solution)) associated with ionization in aqueous solution.

(2) Due largely to electrostatic stabilization by Na^+, the corresponding lowest energy gas-phase IPs of the base, sugar, and phosphate groups in the 5′-dGMP$^-$ cluster are significantly larger than in isolated 5′-dGMP$^-$, and the energetic ordering of the IPs is different.

(3) Differences between values of $\Delta G_{\mathrm{ioniz}}$(solution) for 5′-dGMP$^-$, which is not incorporated into a cluster, versus 5′-dGMP$^-$, which is in clusters, are smaller than corresponding differences in gas-phase IPs. The small differences between values of $\Delta G_{\mathrm{ioniz}}$(solution) occur because the Na^+ electrostatic stabilization, which increases 5′-dGMP$^-$ gas-phase IPs in the clusters, is almost canceled by the relaxation of bulk water which stabilizes the cluster after ionization.

(4) For reaction of nucleoside model compounds with $CH_3N_2^+$, the occurrence of reaction barriers, associated with maxima in the potential energy surfaces relative to minima associated with reactant ion−molecule complexes, is dependent on differences between Gibbs free energies of hydration for the transition states versus the reactant complexes.

(5) Changes in π electron distributions that occur as transition states are approached for 10 different reactions of $CH_3N_2^+$ with nucleoside model compounds provide evidence that DNA methylation and ethylation patterns are significantly influenced by π polarization. This conclusion is consistent with the increase in reactivity which occurs as the base π ionization potentials decrease, and with the selectivity of S_N2 methylating and ethylating reagents toward N7 of guanine.

Acknowledgment. Support of this work by the American Cancer Society (Grant No. CN-37B) and the Petroleum Research Fund (Grant No. 26499-AC) is gratefully acknowledged. Computer access time has been provided by the Computer Center of the University of Illinois at Chicago, the Cornell Theory Center, and the National Center for Supercomputing Applications at the University of Illinois at Urbana-Champaign. The authors would like to thank Professor Arieh Warshel (University of Southern California) for helpful discussions and for making Polaris version 3.2 available for this investigation.

JA953465B

(92) For reaction at N7 of 9-MeG, $\Delta H^{\ddagger}_{gas}$ is negative relative to that of the separated reactants.

(93) (a) Hanlon, S. *Biochem. Biophys. Res. Commun.* **1966**, *23*, 861. (b) Yu, C.; O'Donnell, T. J.; LeBreton, P. R. *J. Phys. Chem.* **1981**, *85*, 3851. (c) Fetzer, S. M.; Huang, C.-R.; Harvey, R. G.; LeBreton, P. R. *J. Phys. Chem.* **1993**, *97*, 2385.